

## Article

# Comparative Assessment of Performance-Based Design Methodologies Applied to a R.C. Shear-Wall Building

Juan C. Vielma-Quintero, Jorge Carvallo and Juan C. Vielma \* 

School of Civil Engineering, Pontificia Universidad Católica de Valparaíso, Valparaíso 2340000, Chile; juan.vielma.q@mail.pucv.cl (J.C.V.-Q.); jorge.carvallo@pucv.cl (J.C.)

\* Correspondence: juan.vielma@pucv.cl; Tel.: +56-332273644

**Abstract:** Performance-based design has been increasingly used in practice due to computational improvements, the sophistication and dissemination of nonlinear analysis methods, and the development of commercial programs that facilitate its use. We can evaluate the nonlinear effects of seismic events of great magnitude on the structural behavior of a building, verify preliminary designs based on force-based methods, validate standard design regulations, determine deformations, and calculate accelerations that can be translated into parameters of structural damage and economic losses, among other functions. Guiding documents have presented methodologies to establish requirements, evaluation criteria, analysis methods, etc., each with different objectives, revealing the lack of a consensus method. In this paper, the state of the art of performance-based design is studied, and some of the most relevant methods, such as ASCE 41-17, ASCE 7-16, and the alternative procedure of ACHISINA, are applied to a structure with shear walls designed according to current Chilean regulations. Additionally, modal-response spectrum analysis is used. The modeling of the earthquake-resistant structure of the building, the preparation of seismic records, and the consideration of aspects that limit the rigorous application of the method are addressed in a nonelastic analysis framework. Results obtained in the respective analyses that are used to evaluate the structural performance are compared with the corresponding performance criteria for each standard, considering the characteristics of each methodology. Moreover, the main complications that can occur during the application of the methods are discussed.

**Keywords:** performance-based design; nonlinear analysis; ASCE 7-16; ASCE 41-17; ACHISINA; shear wall structure



**Citation:** Vielma-Quintero, J.C.; Carvallo, J.; Vielma, J.C. Comparative Assessment of Performance-Based Design Methodologies Applied to a R.C. Shear-Wall Building. *Buildings* **2023**, *13*, 1492. <https://doi.org/10.3390/buildings13061492>

Academic Editors: Asimina Athanatopoulou-Kyriakou and Konstantinos Kostinakis

Received: 8 May 2023

Revised: 6 June 2023

Accepted: 8 June 2023

Published: 9 June 2023



**Copyright:** © 2023 by the authors. Licensee MDPI, Basel, Switzerland. This article is an open access article distributed under the terms and conditions of the Creative Commons Attribution (CC BY) license (<https://creativecommons.org/licenses/by/4.0/>).

## 1. Introduction

Performance-based design emerged from the need of structural designers to rationalize code requirements, which were developed empirically or based on expert judgments, and to supersede these requirements in design by demonstrating equivalent or superior performance [1,2]. This approach serves as a tool that allows for the validation of architectural designs that are noncompliant with code, accommodating the use of new materials and/or innovative structural systems, and exempting the limits of regulations that govern traditional methods, such as the maximum permitted height of a building [3–5]. Additionally, decision makers need to quantify the benefits of investing in a superior seismic-resistant structure and analyze the damages and losses it could suffer during its service life based on its performance [6–11]. Likewise, society is concerned about the safety and reliability of seismic design, seeking to protect the lives of occupants, and to ensure the continuous operation of essential services and secure containment in facilities that handle hazardous elements, among several other specific functions [12–14].

These achievements have been made possible thanks to recent technological improvements such as more complex modelling, due to evolutionary increases in computer processing capacity, and research that resulted in the formulation of enhanced procedures

and analysis methods [15–19], which allowed the migration from empirical considerations and expert experience toward more realistic objective assessments of structural behavior based on the satisfaction of specified performance objectives [20–22].

To carry out this process, various entities and research groups have developed documentation proposing methodologies to assess designs and/or evaluations based on this concept. Moreover, the requirements and considerations of modeling and analysis and the performance objectives that must be considered to satisfy a local or global performance criterion for a given seismic demand must be assessed. However, while these objectives may coincide in the design of a building with predictable and reliable behavior during seismic events, there are differences regarding the desired performance levels [23–26] and evaluation requirements, highlighting the different expectations as to both expected damage for a certain level of seismic demand and the rigor required for analysis.

Consequently, recent publications have sought to regulate and standardize the implementation of the method, seeking to integrate the results of new research and incorporating the relevant criteria. In this context, the particularities of the guides and procedures widely used today are addressed, among which ASCE 7-16 [27], ASCE/SEI 41-17 [28], TBI [29], LATBSDC [30], and FEMA P-58 [31] stand out. It is worth noting that it is not within the scope of this article to fully address the contents of these procedures, so interested readers are referred to the following articles for further detail: [32–35]. It is also worth noting that performance-based design is already being used to optimize both structural configurations [36] and the distribution of reinforcement steel [37].

Performance-based design has gradually become associated with European standards governing the seismic design of buildings [38] in the context of structural engineering. The main purpose has been twofold: firstly, to establish improvements to seismic design factors [39–43] based on the application of specific limit states, and secondly, to explore new alternatives for optimizing the design of both reinforced concrete and steel structures [44–46]. Meanwhile, other studies have focused on identifying the needs that would emerge if performance-based design were to be implemented [47,48]. However, due to the limited scope of this work, the utilization of European standards to compare performance-based design practices in Chile has not been taken into consideration, although it is recommended that they be considered in future studies that expand on these aspects. As an alternative to the normative procedures employed in this study, it is suggested that recently developed procedures based on the combined study of demand and capacity uncertainties [49] be considered.

This study presents the results of a seismic-behavior analysis of a building with reinforced concrete shear walls designed according to force-based design (FBD) and performance-based design (PBD) code procedures. We first provide a brief background of the primary PBD building codes used worldwide. Then, we describe the methodology applied, defining the case study and its main characteristics. Throughout the study, we compare the performance of applying American codes with the procedure used in Chile, and finally, we present a summary of the impact of PBD on the increase in the materials used in the studied structure.

## 2. Background

### 2.1. ASCE 7-16

The ASCE-7 code, first published in 1988 by the American Society of Civil Engineers (ASCE), describes the procedure for determining minimum loads (dead, live, wind, and snow, among others) and their combinations, as well as the seismic risk to be used for the design of structures. When combined with material design specifications, the provisions of this code are intended to provide the level of performance for which it was developed.

In its latest edition, ASCE7-16, the code presents a methodological framework to achieve this objective, in which the design must comply with the applicable requirements of the code, except for those in which it is permitted to use the performance-based design criteria in Section 1.3. This can include the response history analysis (RHA) method in

Chapter 16, directly adapted from FEMA 273 procedures, consisting of two code-level evaluations: design basis earthquake (DBE), and maximum considered earthquake (MCE). The DBE evaluation aims to establish minimum stiffness and strength requirements according to the code regulations in Chapter 12 using a linear RHA analysis. In contrast, the MCE evaluation considers a nonlinear RHA analysis to demonstrate the stable and predictable behavior of the structure, verifying deformations in ductile elements, and forces in fragile elements. It is worth noting that this method is only valid for the design of new buildings, with ASCE 41-17 being the code for evaluating the performance of existing buildings.

## 2.2. ASCE/SEI 41-17

In 2006, the ASCE, based on the previous document FEMA 273/356, published the ASCE/SEI 41-06 standard, which seeks to standardize the use of performance-based design concepts for the seismic evaluation of existing buildings. In its latest version, dated 2017, it presents a close relation to ASCE 7-16. In the latter, alternative methods such as performance-based design (according to Section 1.3.1.3) are allowed if a structure's viability is ensured with the same reliability as that provided by traditional methods. In other words, the performance objectives of ASCE 41-17 are linked to those of ASCE 7-16, which are classified as follows:

- Basic performance objectives for existing buildings (BPOE): Standard performance objective for existing buildings, according to the building risk category as defined in ASCE 7.
- Basic performance objective equivalent to new building standards (BPON): Improved performance objective, with the scope of providing the same performance as new buildings designed by ASCE 7.
- Enhanced performance objectives: Higher performance objectives than BPOE, achieved by increasing the building risk category, seismic hazard, structural and/or nonstructural performance level, or any combination of the above.
- Limited performance objectives: Lower performance objectives than BPOE, achieved by decreasing the building risk category, seismic hazard, structural and/or nonstructural performance level, or any combination of the above.

The three main structural performance levels are Immediate Occupancy (IO), Life Safety (LS), and Collapse Prevention (CP); there are two complementary levels called Damage Control and Limited Safety. Similarly, the document evaluates the performance of nonstructural elements, defining five discrete levels, as: Operational, Position Retention, Life Safety, Reduced Hazard, and 'Not Considered'.

## 2.3. PEER TBI and LATBSDC Alternative Procedure

In 2010, the Tall Building Initiative of the Pacific Earthquake Engineering Research Center (PEER) produced a document summarizing the recommended process for designing and evaluating tall buildings located in high seismic hazard zones. In its current 2020 version, detailed guidelines are presented for designs for Serviceability Limit State (Serviceability Level) and Life Safety (MCE Level). The Serviceability level is characterized by the seismic demand obtained from a modal-response spectrum analysis or linear dynamic analysis in a three-dimensional model, considering a uniform hazard spectrum (UHS), with a return period of 43 years and a damping value of 2.5%.

Similarly, the Los Angeles Tall Building Structural Design Council (LATBSDC) developed a design guide, first published in 2005, with the purpose of presenting an alternative procedure for designing tall buildings in the Los Angeles region, while also allowing its use in the design of other types of buildings. In the latest version, from 2020, its similarity to the PEER TBI is emphasized regarding the guidelines and format, but there are some differences, mainly in its definition of tall buildings, modeling and analysis considerations, and acceptance criteria.

#### 2.4. ACHISINA Performance-Based Seismic Design Procedure

Currently, the seismic design code in Chile is characterized by requiring only the use of elastic linear analysis, with the response spectrum method being the most prevalent. The use of nonlinear static analysis with incremental pushover is not prescribed by the main seismic codes (except the EC-8), but it is usually used to support the reviews of residential high-rise buildings. On the other hand, nonlinear dynamic time history analyses are rarely used, and are mainly employed to verify the seismic response of buildings with supplemental dissipation.

Despite empirical validations of the expected performance level by recent seismic events, the need arose to establish a formalized analysis method to explicitly validate Chilean designs [50]. A document containing the performance-based design procedure by ACHISINA [51] was developed by consensus, with the purposes of its being discussed, evaluated and subsequently used as a standard in the future.

### 3. Methodology

To develop the performance evaluation of a building under study, it is necessary to define the methodology for modeling and analyzing the seismic-resistant structure following the guidelines and recommendations contained in the codes that relate to performance-based design, as briefly explained in the previous section. It is important to emphasize that the application of this methodology requires existing advanced knowledge of structural engineering to accurately represent the expected behavior through a computational model, defining the properties of materials and elements, as well as their interactions. Similarly, it is equally relevant to prudently establish the conditions and parameters with which the nonlinear analysis will be carried out, taking into consideration the types of results and the needed precision without sacrificing the possibility of achieving convergence.

In this context, the methodological framework used to evaluate the performance of a building structure based on walls, through nonlinear static and dynamic analysis, is presented under the procedure stipulated in the ASCE 7-16, ASCE 41-17, and ACHISINA documents.

#### 3.1. Building Description

The building analyzed consists of a residential apartment tower located in Viña del Mar, Chile. The building is constructed with reinforced concrete and has 14 stories and two basement levels, totaling a height of 37 m from the ground level. The building is founded on soil type C and is located in seismic zone 3 (effective acceleration  $A_0 = 0.4 g$ ), with an occupancy category II, as classified by the NCh433 code.

In terms of its structural system, although following the Chilean practice of using special walls with complex geometries and coupling beams, the building does not have a large number of shear walls distributed on each story, as shown in Figures 1 and 2. Additionally, the number of perimeter beams is noteworthy compared to other buildings, which have a more balanced combination of walls and beams in their perimeter. As to their dimensions, the wall thicknesses vary per story and direction. In the Y direction, thicknesses of 30 cm, 25 cm, and 20 cm are generally used for stories 1–2, 3–4, and 5–14, respectively. On the other hand, in the X direction, the thickness is generally 20 cm for all stories. Moreover, the beams generally have dimensions of 65 cm in height and 20 cm in width for all stories.

The structural design was carried out using a modal-response spectrum analysis according to the provisions of the NCh433 standard, following the ACI 318-08 design code [52]. During this process, the reinforcement detailing of the walls and beams was performed using A630-420H grade steel, and the concrete grade to be used was established. Grades G35, G30, and G25 were used for the base and first story, stories 2–3, and stories 4–14, respectively. The results of the analysis can be summarized in Table 1 for both orthogonal directions.

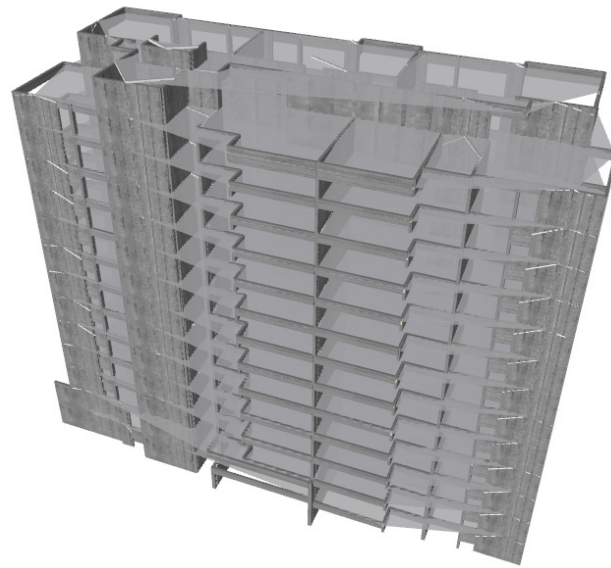


Figure 1. Perspective view of the computational model of the building under study.

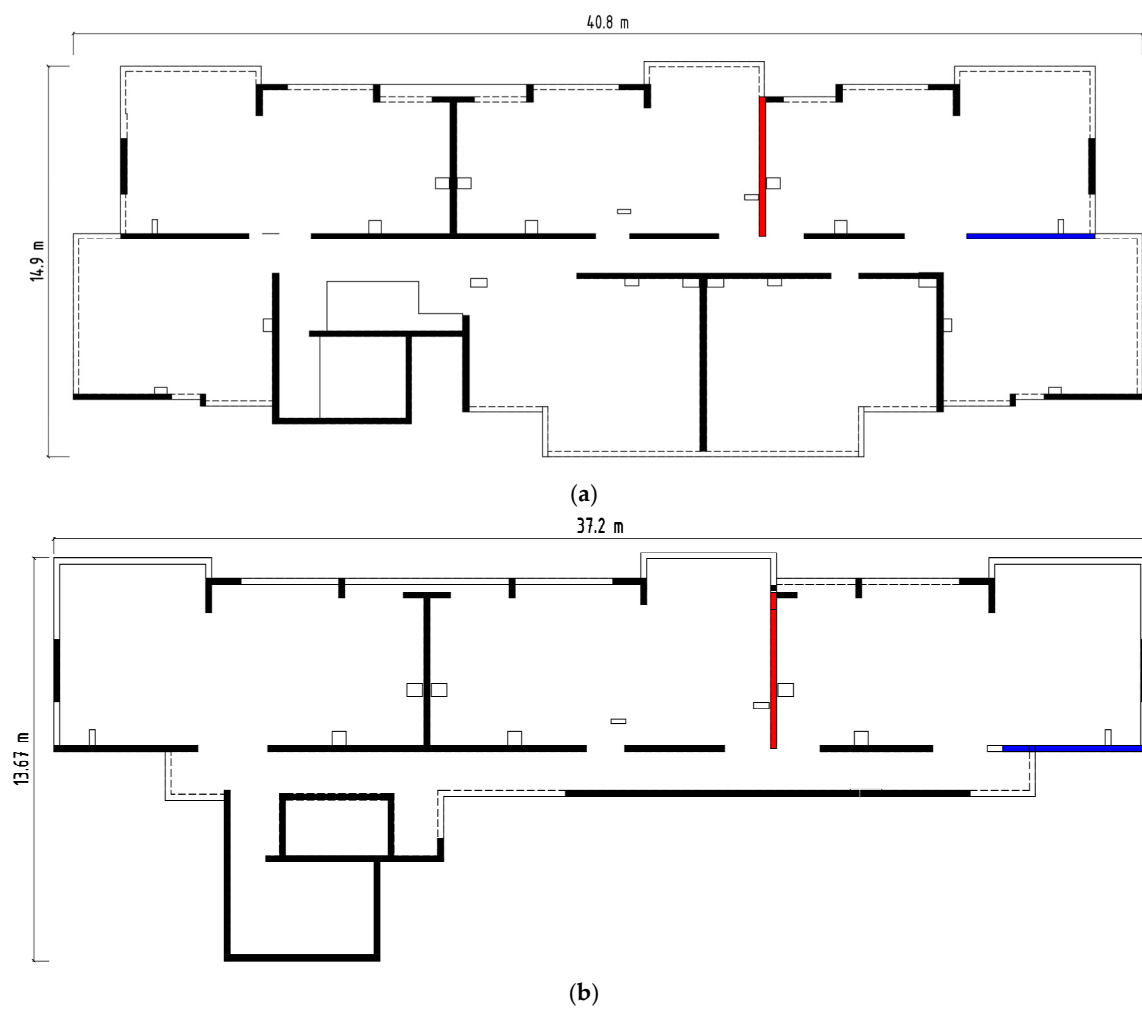


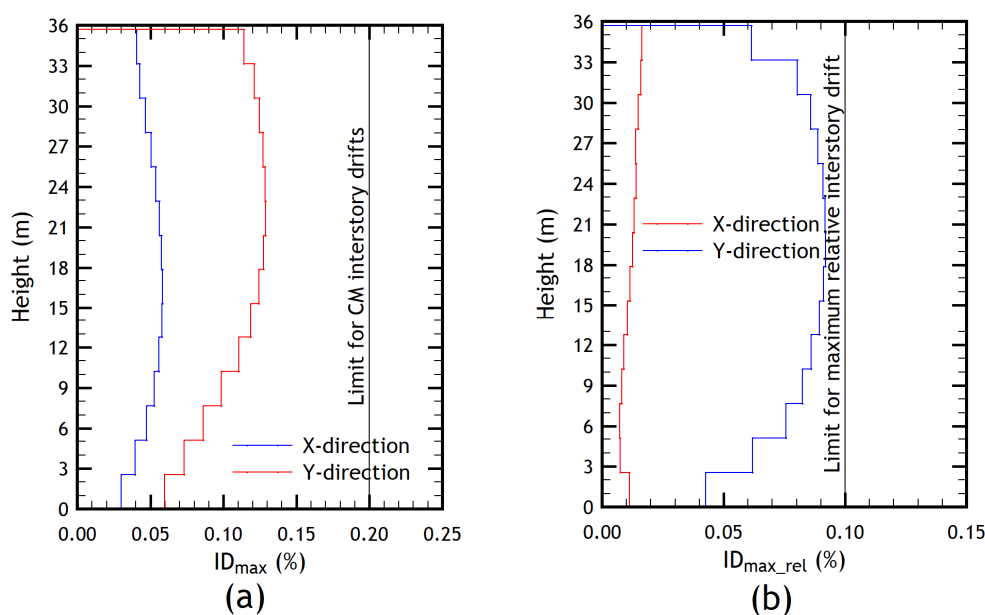
Figure 2. Structural plan, with black lines marking the walls and light lines marking the beams: (a) Typical floor, and (b) Roof floor.

**Table 1.** Results of the modal-response spectral analysis.

Parameter	X-Direction	Y-Direction
Analysis fundamental period [s]	0.86	1.41
Response reduction factor $R^*$	8.26	9.39
Elastic base shear $Q_{(R=1)}$ [kN]	28,941.95	18,449.57
Maximum inelastic base shear $Q_{max}$ [kN]	12,506.38	12,506.38
Minimum inelastic base shear $Q_{min}$ [kN]	5955.45	5955.45
Computed inelastic base shear $Q_{(R^*)}$ [kN]	3502.76	1965.53
Inelastic design base shear $Q_{design}$ [kN]	5955.45	5955.45
Adjusted response reduction factor $R^{**}$	4.86	3.10
Inelastic spectral acceleration $S_a$ [ $m/s^2$ ]	6.23	3.20
Inelastic spectral displacement $S_{de}$ [m]	0.1211	0.2199
Computed ultimate displacement $\delta_u$ [m]	0.1574	0.2859

Although not currently required by regulations, during this process, capacity design principles for the walls were considered, principles which were not included until the 2019 edition of the ACI318 code [53].

The force-based design has been carried out by applying regulatory provisions that include the definition of inelastic design spectra for each orthogonal direction of the structure. It should be noted that the structuring has been carried out in order to obtain a regular-response structure. To achieve this, the Chilean seismic regulations present two important verifications based on interstory drifts. The first verification is performed on the interstory drifts calculated at the center of mass of each floor, which should not exceed 0.2%, ensuring regularity in elevation. On the other hand, it must be ensured that the difference in interstory drifts between the center of gravity of each floor and the interstory drift of the most unfavorable point of that same floor does not exceed the value of 0.1%, which guarantees the regularity-in-plan of the building. Figure 3a,b show compliance with both regulatory provisions. It should be noted that the Chilean regulations calculate interstory drifts based on displacements directly calculated using the inelastic design spectrum, without amplifying them by the response reduction factor or any function dependent on it.

**Figure 3.** Criteria used to verify the structural regularity for (a) CM interstory drift, and (b) interstory drift between the CM and the most unfavorable point of the floor.

### 3.2. Structural Modelling

The non-linear modeling of the earthquake-resistant structure of the building under study, as shown in Figure 1, was carried out using the tools and options provided by the Seismostruct [54] and Seismobuild [55] software products, following the recommendations and guidelines presented in their documentation. The following section presents the manner in which the programs model the structural elements and their theoretical basis, as well as the considerations used for the development of the analytical model.

Firstly, in the modeling process, geometric nonlinearity is considered by taking into account large displacements and rotations, as well as independent chord deformations of the element (P-Delta effects). Secondly, material nonlinearity is accounted for by the complete distribution of inelasticity in the element, as opposed to the usual practice of using models where plasticity is concentrated in specific points. This has the advantage of not requiring empirical calibration of the actual or ideal behavior of the element under idealized load conditions, as is the case with concentrated plasticity models. Fiber-based modeling is used to represent the cross-sectional behavior of the element, in which each fiber is associated with a uniaxial stress–strain relationship, and the state of the element is obtained from the integration of the nonlinear uniaxial stress–strain response of each individual fiber into which the section is subdivided (the number of fibers depends on the dimensions of the cross-section of each structural member).

These elements with complete inelasticity distribution can be implemented using two different finite-element formulations: the classic displacement-based finite elements (DB) and the more recent force-based (FB) elements. In the first formulation, the procedure consists of imposing a displacement field, such as the linear variation of curvature in the member. In contrast, in the second formulation, the equilibrium of the element is strictly fulfilled without preventing the development of inelastic deformations in the member. Based on this, each member of the structure is defined as a single element (beam type), with walls established as FB elements and beams as DB elements, according to the program manual recommendations. For this, the geometric parameters, materials used, and reinforcement detailing corresponding to the member must be tabulated, seeking to emulate as closely as possible the real arrangement of the structural members of the building under study. To avoid artificially flexible models, walls include rigid offsets that are applied to the beams linked to them. Reinforced concrete slabs are modeled as rigid diaphragms.

After defining the elements and modeling the structural system of the building, the model must be verified to assess its validity. In this case, the fiber-based wall and beam response under a pushover is compared with their respective force-based-design idealized counterpart, disregarding the effect of stiffness degradation under cyclic loading. Under this process, the moment–curvature relationship of the walls and beams is examined, where it displays good agreement between the two models, both in their relationship curves and maximum compressive strain obtained. However, the complete list of details on which the verification is made is not within the scope of this article. In this case, as to readers interested in how to organize the information of the structural model and its verification, it is recommended that they the work of Cao et al. [56].

Finally, energy dissipation due to damping is included in the model by taking into account the hysteretic cycles of the previously-established constitutive models. However, the ACHISINA document and the prescriptions of ASCE 7-16 nonlinear analysis allow the inclusion of an equivalent viscous or proportional damping in mass and stiffness (Rayleigh), with a maximum value of 2.5% of critical damping in the principal modes. All of this is performed to represent the inherent damping of the structure, including various sources other than hysteresis, such as friction and the presence of non-structural elements, among others.

### 3.3. Material Properties

To model the building, it is necessary to define the parameters of the materials that will be assigned to the elements that make up the structure. Because nonlinear behavior will be analyzed, it is necessary to establish constitutive relationships that include the effect of the degradation of material strength [57]. For this purpose, the software programs Seismostruct and Seismobuild include a list of varied constitutive models for steel and concrete which allow for the variation of parameters defining the shape of the curve and the specific weight of the material. For concrete, the nonlinear constitutive model of Mander et al. [58] is used. The parameters defining the constitutive model are summarized in Table 2 for the concrete grades used in the model. For the longitudinal and transverse reinforcing steel, the Menegotto and Pinto constitutive model is employed [59] for the steel grades indicated in Table 3.

**Table 2.** Constitutive model parameters by Mander et al. for concrete grades G25, G30 and G35.

Parameter	Concrete G25	Concrete G30	Concrete G35
Compression strength (MPa)	33.00	38.00	43.00
Strength lower bound (MPa)	25.00	30.00	35.00
Tension strength (MPa)	2.60	2.90	3.20
Modulus of elasticity (MPa)	26,999.00	28,973.00	30,820.00
Specific weight (kN/m <sup>3</sup> )	24.00	24.00	24.00

**Table 3.** Constitutive model parameters by Menegotto and Pinto for steel grade A630-420H.

Parameter	Value
Modulus of elasticity $E$ (MPa)	200,000.00
Yield strength $F_y$ (MPa)	490.00
Strain hardening parameter (Dimensionless)	0.0050
Transition curve initial shape parameter (Dimensionless)	20.00
Transition curve shape calibrating coefficient A1 (Dimensionless)	18.50
Transition curve shape calibrating coefficient A2 (Dimensionless)	0.15
Transition curve shape calibrating coefficient A3 (Dimensionless)	0.00
Transition curve shape calibrating coefficient A4 (Dimensionless)	1.00
Fracture/buckling strain (Dimensionless)	1.00
Specific weight (kN/m <sup>3</sup> )	78.00

### 3.4. ASCE 41-17 Performance-Based Analysis Method

#### 3.4.1. Seismic Record Selection and Adjustment

As to the four seismic hazard levels contemplated in the BPOE, the same number of objective response spectra must be developed for each one; their ordinates will be used to adjust the seismic records that will be used in the analysis. Table 4 displays the four levels of hazard defined by the corresponding exceedance probabilities for a 50-year lifespan and its associated return period. In addition, the target performance levels for each hazard level are shown.

**Table 4.** Seismic hazard levels and the corresponding target building performance levels defined according to ASCE 41-17.

	Target Building Performance Level					
	Eceedance Probability	Return Period (Years)	Operational Level	Immediate Occupancy	Life Safety	Collapse Prevention
Seismic hazard	50% in 50 years	72	x			
	10% in 50 years	225		x		
	5% in 50 years	975			x	
	2% in 50 years	2475				x

Due to the need to modify the records for these four spectra, it was decided to use artificial records, which is permitted by ASCE 7-16 in Section 16.2.2, as it is consistent with the magnitudes and other variables that condition the seismic demand. From this, 11 pairs of records are generated as required by ASCE 41-17 for each orthogonal direction of the building. An example of these is shown in Figure 4a, the response spectra of which are appropriately adjusted to the target design spectrum, as evidenced in Figure 4b. In particular, the artificial earthquakes have been generated using the procedure of Al Atik and Abrahamson [60]. According to the recent work by Cao et al. [61], an algorithm developed by these authors can be used in order to obtain stochastic accelerograms to perform structural fragility analysis.

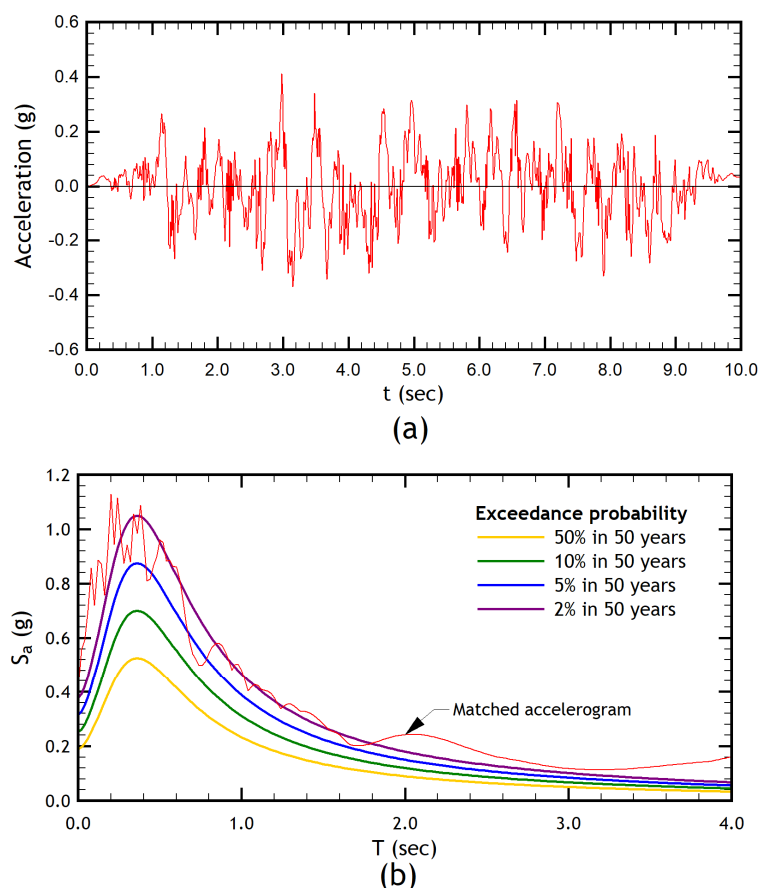


**Figure 4.** (a) Example of artificial accelerogram. (b) Adjustment of the matched acceleration spectrum.

### 3.4.2. Acceptance Criteria

The ASCE 41-17 document provides acceptance criteria for the different building materials and types of structural systems utilized. For structures based on reinforced-concrete coupling walls and beams, the criteria are established in accordance with the provisions of Section 10.7. In general, the acceptance criteria correspond to the allowable deformation capacity of the elements for a given performance level, distinguishing between those controlled by bending or shear. For elements controlled by bending, such as walls or beams, the engineering parameter of interest is the chord rotation, while for walls, the equivalent parameter is the plastic hinge rotation. For elements controlled by shear, beams also use chord rotation, while walls are evaluated based on the interstory drift.

### 3.5. ACHISINA Performance-Based Analysis Method

The procedure outlined in the ACHISINA document [51] includes the performance evaluation of the structure for two limit states: Immediate Occupancy and Additional Deformation Capacity, which are comparable to the Immediate Occupancy and Collapse

Prevention levels of other standards. To carry out these evaluations, the use of nonlinear dynamic time history analysis is required for both limit states, with allowance made for the alternative use of pushover analysis for preventing collapse. For the purposes of this article, the use of this procedure will be focused on the development of dynamic analysis for both limit states, and the seismic records and acceptance criteria used will be detailed in the following sections.

### 3.6. Building Modeling

One crucial step toward developing the methodology is the nonlinear modeling of the structure, as the quality of the results obtained depends highly on the accuracy of capturing the behavior of the structure under the imposed loads. In the following section, the relevant characteristics of the building under study will be described, followed by the definition of the materials according to their parameters and constitutive models. Finally, important considerations for modeling each element and other relevant aspects will be discussed to obtain the computational model necessary for the analysis, as illustrated in Figure 1.

#### 3.6.1. Seismic Record Selection and Adjustment

Seismic records are selected according to the requirements of the ACHISINA document, which states that a minimum of 3 pairs of horizontal records (real or artificial) with congruent characteristics (source, soil type, and magnitude, among others) regarding the events controlling the design seismicity in the region must be used. To achieve this, the Chilean records presented in Table 5, obtained from the Center for Engineering Strong Motion Data (CESMD) [62] database, were chosen to obtain several record pairs greater than 7; the average value of the parameter of interest evaluated in the acceptance criteria was used.

**Table 5.** Descriptive summary of Chilean records used.

Earthquake	Date	Magnitude ( $M_w$ )	Station	Epicentral Distance (km)	Component	PGA (cm/s <sup>2</sup> )
Maule	27 February 2010	8.8	Angol	209	E-W	684
					N-S	916
Maule	27 February 2010	8.8	Concepción San Pedro	109	97	598
					7	667
Maule	27 February 2010	8.8	Constitución	70	E-W	530
					N-S	618
Maule	27 February 2010	8.8	Llolleo	274	E-W	324
					N-S	549
Maule	27 February 2010	8.8	Santiago Maipú	69	E-W	481
					N-S	549
Coquimbo	16 September 2015	8.3	El pedregal	92	90	677
					360	561
Coquimbo	16 September 2015	8.3	Tololo	175	90	234
					360	338
Coquimbo	16 September 2015	8.3	San Esteban	168	90	268
					360	182
Puerto Quellón	25 December 2016	7.6	Loncomilla	136	90	136
					360	148
Puerto Quellón	25 December 2016	7.6	Hotel Espejo de Luna	75	90	371
					360	350
Valparaíso	24 July 2015	6.9	Torpederas	39	90	889
					360	731

Additionally, these seismic records must be modified so that the average of the combined displacement spectra by SRSS of all pairs is not less than 1.17 times the elastic displacement spectrum of NCh433, considering  $\beta = 5\%$ , between the periods of  $0.50 T$  and  $1.25 T$ , where  $T$  corresponds to the principal periods. However, despite this indication, the accelerograms have been matched for a range of periods between 0.05 s and 4.00 s. (see Figure 5a,b). This consideration is pertinent, as it incorporates seismic demands for the range of short periods, which correspond to higher modes of vibration. The contribution

of these higher modes of vibration becomes decisive in buildings of certain height. To effectively control the computational cost of the analyses, the records are trimmed using the significant duration criterion of the records, as defined by Arias intensity [63].

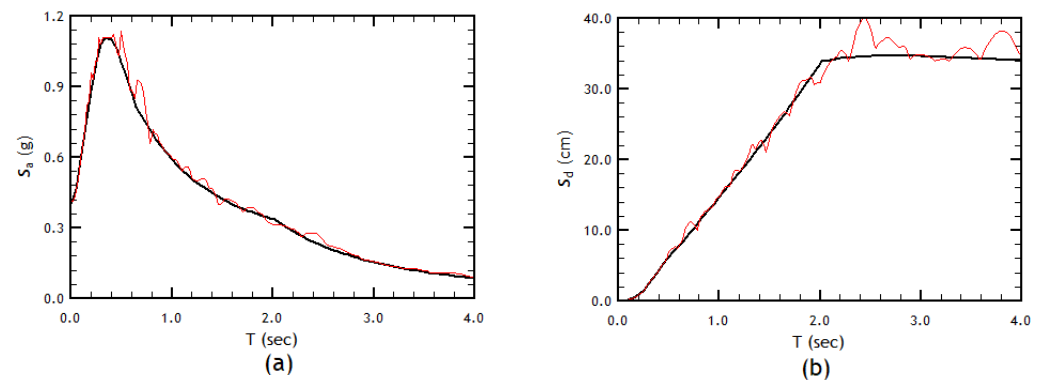


**Figure 5.** Correspondence of the response spectrum of the matched record with respect to the acceleration spectrum derived from the design spectrum in soil displacement C amplified by 17%: (a) acceleration spectra; (b) displacement spectra.

Finally, the spectral matching procedure is used to modify the corrected records so that the combined displacement spectra are not less than the displacement spectrum defined in the requirements of the ACHISINA document. This process is facilitated by the Seismomatch program [64], in which a group of records can be matched based on an objective acceleration record. However, since the document requires adjustment of the displacement spectrum, the resulting acceleration spectrum from the integration is used instead. The matching is shown in Figure 5a,b for the acceleration and displacement spectra, respectively.

From this entire procedure, modified records can be obtained for use in the Serviceability limit state, corresponding to the design earthquake (DE) in the ACHISINA document. For the maximum considered earthquake (MCE), the norm allows the use of the same historical records used as the design earthquake, but with their accelerations increased by 30%.

### 3.6.2. Acceptance Criteria

To assess the performance level of the building, the procedure outlined in the ACHISINA document includes performance criteria for both limit states, with verification carried out both at the global level and for the individual structural elements. For the case study, it is of interest to understand the performance criteria for the walls and coupling beams controlled by deformation, which can be summarized in Table 6.

**Table 6.** Acceptance criteria according ACHISINA's manual for the Immediate Occupancy and Additional Deformation limit states.

Criteria Type	Criteria	Limit Value	
		Immediate Occupancy	Additional Deformation
Local	Compression unit strain in confined concrete walls	0.008	0.015
	Compression unit strain in unconfined concrete walls	0.003	0.003
	Tension unit strain in reinforcement steel of walls	0.030	0.050
	Plastic rotation of coupling beams	0.01	No limit if it does not compromise the stability
Global	Story drifts of buildings with fragile nonstructural elements	0.005	No limit
	Story drifts of buildings with ductile nonstructural elements	0.007	No limit

## 4. Results and Discussion

In this section, the results obtained for both static and dynamic nonlinear procedures are presented, using the methodological framework outlined in the previous chapter for their development. The performance criteria governing the evaluation of the studied structure are also discussed. It is impractical within the scope of this article to include a comprehensive evaluation of each element, due to the large number of elements that make up the structure. Therefore, it has been instead decided to include the results of a characteristic wall in each direction, marked in blue and red on the plan, for the X and Y directions, respectively, as shown in Figure 2. These were chosen because they are among the most demanding elements in terms of demand-to-capacity ratios observed in the analyses conducted. Based on this, the results obtained for the three types of analyses considered are shown, discussing the behavior evidenced for the structure, and making a comparison of both performance evaluation methods.

### 4.1. ASCE 41-17 Analysis Results

#### 4.1.1. Pushover Analysis

First, the deformation capacity of the structure under study is determined through nonlinear static analysis, applying a first-mode load pattern (triangular) in each direction, using displacement control. The results obtained, the generated capacity curve in the analysis, and the idealized three-point curve [65] are shown in Figure 6. In addition, the objective displacements are determined for each limit state according to the procedure outlined in Section 7.4.4.3 of ASCE 41-17 [28], with the obtained parameters presented in Tables 7 and 8, located on the capacity curve obtained in the analyses.

In Tables 7 and 8,  $T_e$  represents the elastic period of the building and  $S_a$  the inelastic spectral acceleration, and  $C_0$  is the coefficient that compares the displacement obtained in an SDOF with an MDOF,  $C_1$  is the coefficient that relates the expected inelastic behavior and the elastic response, and  $C_2$  is the coefficient that represents the effect of the degradation of the expected resistance and stiffness in the hysteretic cycles due to the maximum displacement.

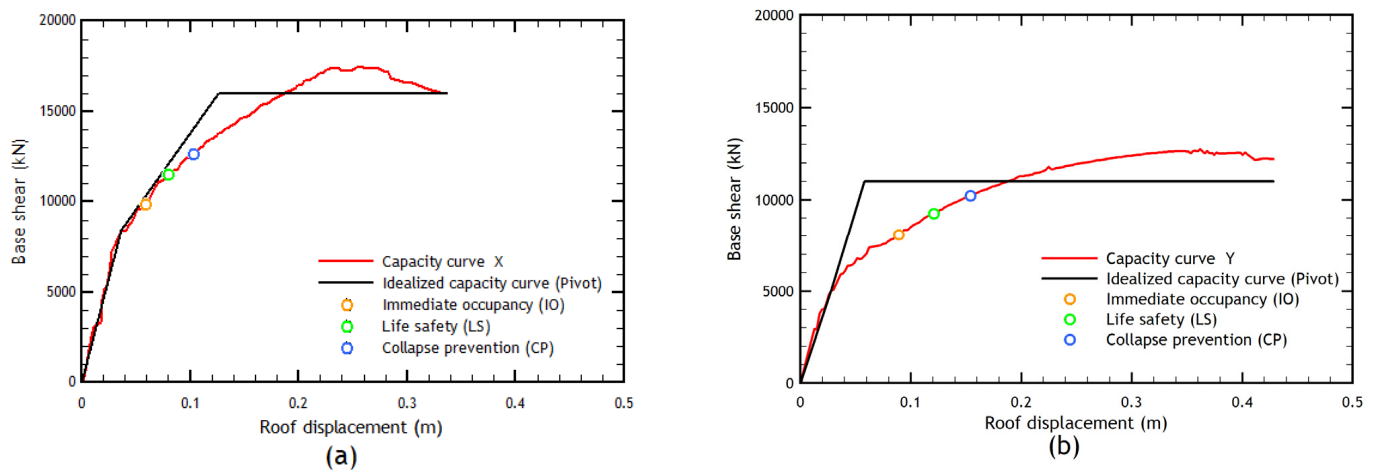


Figure 6. Results of the pushover analysis in the (a) X and (b) Y directions.

Table 7. Parameters obtained for the calculation of the target displacements, X direction.

Limit State	IO	LS	CP
$T_e$ (s)	0.5697	0.5697	0.5697
$S_a$ (g)	0.5783	0.7710	0.9638
$C_0$	1.3000	1.3000	1.3000
$C_1$	1.0682	1.1082	1.1480
$C_2$	1.0068	1.0171	1.0320
Target displacement $\delta_t$ (m)	0.0652	0.0911	0.1197

**Table 8.** Parameters obtained for the calculation of the target displacements, Y direction.

Limit State	IO	LS	CP
$T_e$ (s)	0.8134	0.8134	0.8134
$S_a$ (g)	0.4020	0.5360	0.6700
$C_0$	1.3000	1.3000	1.3000
$C_1$	1.0340	1.0537	1.0735
$C_2$	1.0000	1.0000	1.0000
Target displacement $\delta_t$ (m)	0.0888	0.1207	0.1537

It can be observed that, for the X direction of the analysis, the building can achieve a roof displacement corresponding to 33 cm, and it achieves approximately 43 cm in the Y direction. On the other hand, for both directions, yielding occurs after 4 cm of displacement, and according to the idealized curves, a fully plastic behavior begins, starting from 13 cm and 6 cm for the X and Y directions, respectively. For the target displacements, it can be observed for the X direction that the three performance levels are reached when the structure exhibits a response prior to yielding for values of 6.52, 9.11, and 11.97 cm. In contrast, for the Y direction, performance levels are achieved in plastic behavior, seen in the idealized curve, for displacements of 8.88, 12.07, and 15.37 cm. Figure 7 displays the deformed structure when it reaches the ultimate displacement during the pushover analysis in both X and Y directions. The yellow-colored structural members exceeding the pre-established limit for chord rotation are shown in this figure.

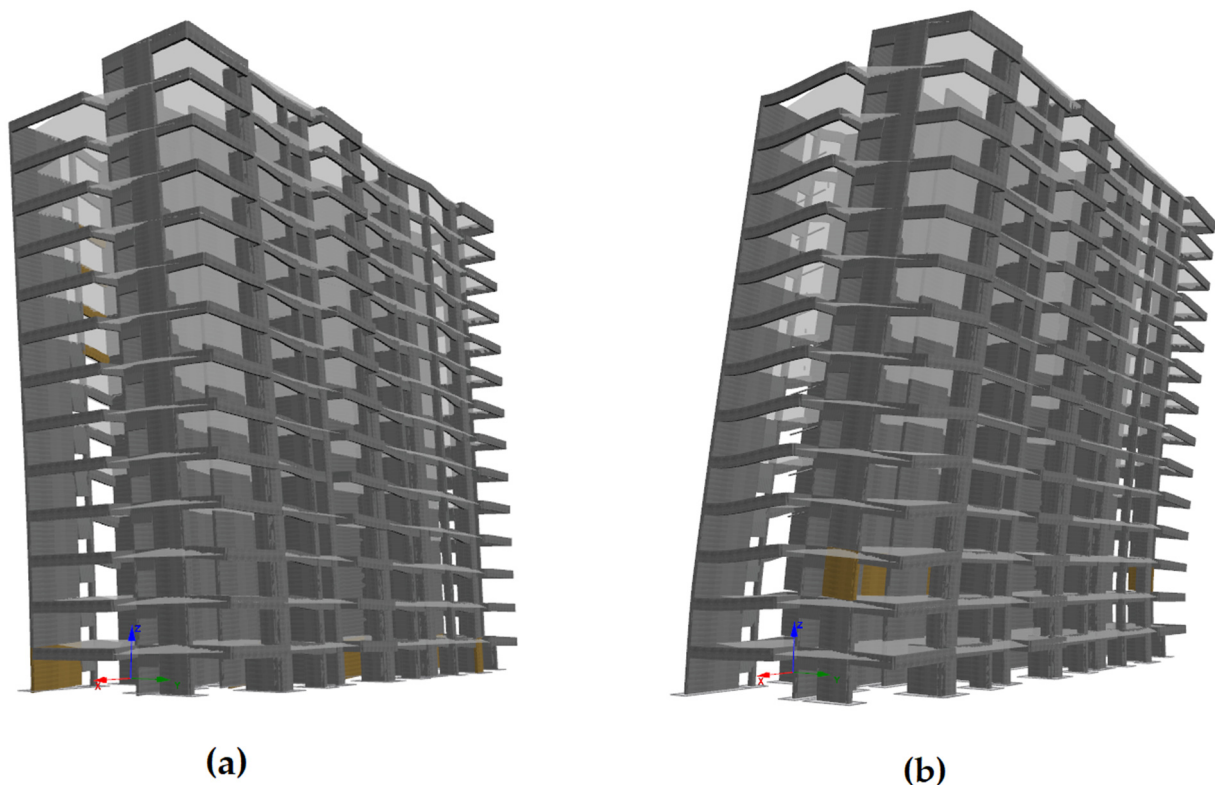


**Figure 7.** Deformed shape of the building during pushover analysis in (a) X and (b) Y directions. Colored members indicate the presence of chord rotations over their limit values for Life Safety.

#### 4.1.2. Nonlinear Dynamic Time History Analysis Results

Starting with the overall performance, the results obtained from the maximum displacements measured at the center of mass are presented in Figure 8, and the interstory drift values measured for each level for the synthetic records of the Collapse Prevention limit state according to ASCE 41-17 are shown in Figure 9. For performance evaluation,

both the value obtained for each individual record and the resulting average are considered, comparing the drift values with the limits established by ASCE 41-17 and the current version of the LATBSDC.

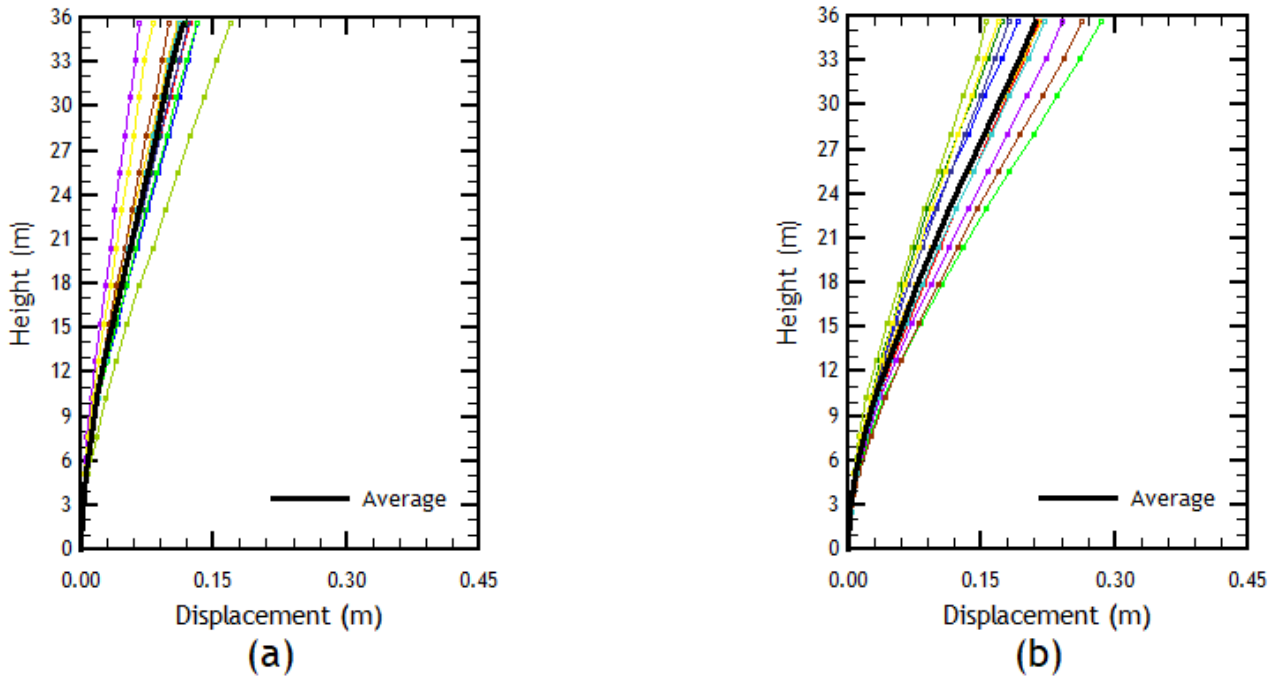


Figure 8. Floor displacements: (a) X direction; (b) Y direction.

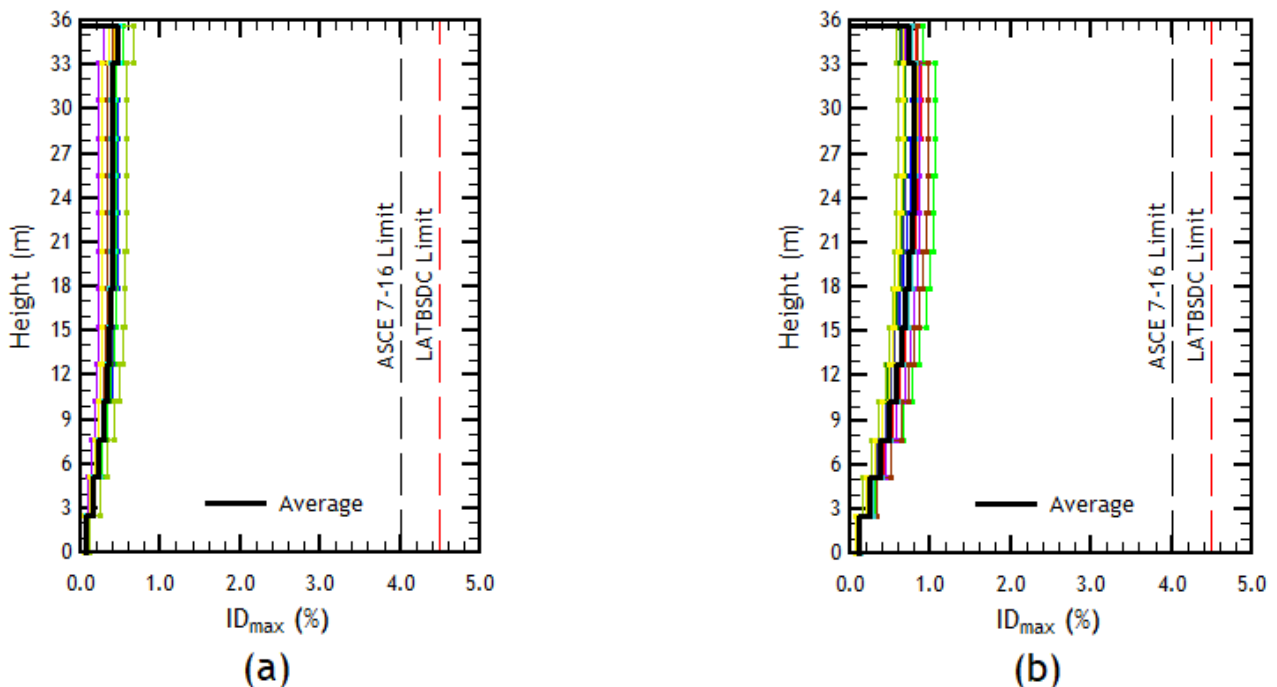
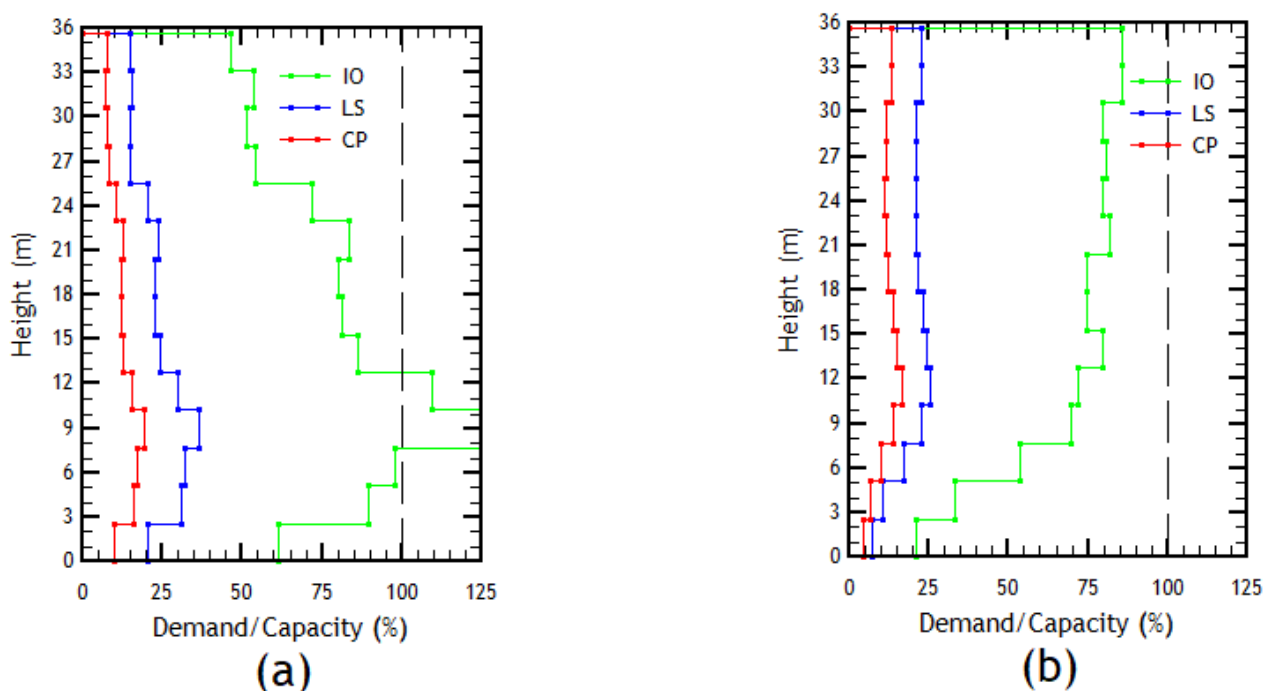


Figure 9. Story drifts: (a) X direction; (b) Y direction.

According to both methodologies, the structure exhibits adequate global behavior, by a considerable margin not exceeding the limits established by both documents. This can be partially attributed to the high stiffness of Chilean structures compared to what is expected in the United States, where the use of frame buildings is common, which are generally more flexible than wall-structured buildings.

Another point of interest is the displacements, where values of 11.53 cm and 21.05 cm are obtained for the X and Y directions at the roof level, respectively. These values are slightly low, compared to the values used for structural design according to NCh433, highlighting the difference in the applied analysis loads. Moreover, it is worth noting that both maximum displacements exceed the Collapse Prevention point obtained in the pushover analysis, even though no elements show failure at this limit state. Therefore, the calculation of the coefficients that determine the target displacement for each of the limit states considered in the pushover analysis should be reevaluated, as presented previously in Tables 5 and 6.

The local performance evaluation of the selected walls is presented in the demand/capacity ratio for chord rotation in Figure 10.



**Figure 10.** Chord rotation demand/capacity ratio: (a) wall in the X direction; (b) wall in the Y direction.

For the values obtained from the chord rotation, good performance is observed for the Life Safety (LS) and Collapse Prevention (CP) limit states. In the case of the X direction wall, the allowed deformation capacity is exceeded for the Immediate Occupancy (IO) limit state for levels 4 and 5. However, for the Y direction wall, the deformation capacity is not exceeded for any of the three limit states. For both directions, the IO limit state represents the most demanding performance level, in that it considers the acceptable rotation values presented in Tables 10–19 of ASCE 41-17 [28], unlike the other limit states.

#### 4.2. ACHISINA Nonlinear Dynamic Time History Analysis Results

For the analysis stipulated by ACHISINA, this section presents the main results obtained corresponding to the global behavior of the structure and the local behavior of the selected wall elements, separated according to the two established limit states of Immediate Occupancy and Additional Deformation Capacity. To evaluate the global performance, as in the previous procedure, displacements are calculated at the center of mass for each level. However, for global performance, it is necessary to discretize deformations by material type, as indicated in the methodological framework. To perform this, the fibers are selected as illustrated in Figure 11, choosing the outermost fiber corresponding to the steel element (Figure 11a), edge element (Figure 11b), and double mesh (Figure 11c).

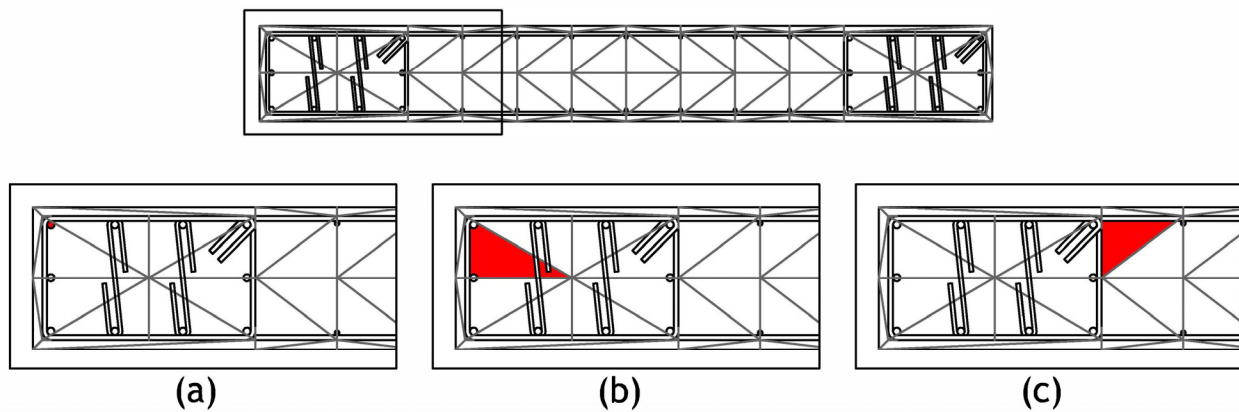


**Figure 11.** Location of fibers for local performance evaluation, wall in X direction: (a) reinforcement steel; (b) concrete in edge element; and (c) concrete in double mesh.

#### 4.2.1. Immediate Occupancy Limit State Results

First, Figure 12 shows the maximum displacement computed for the center of mass of each level. Figure 13 presents the interstory drifts, which show the average and individual values for each orthogonal direction of the structure.

For the global performance assessment, the limit corresponding to ductile nonstructural elements is considered, which, for the procedure, represents a maximum value of 0.7% for interstory drift. Based on this, it can be observed that for the X direction, this criterion is satisfactorily met. However, there are concerns at the fourth story and above for the Y direction, which reach values of 1% of the interstory height. This is due to the high flexibility exhibited by the building in this direction.

It is also interesting to compare the displacements and interstory drifts resulting from the application of both methods, as shown in Figures 14 and 15, for the comparison between both parameters. Note the conservative nature of the application of the ACHISINA manual, since both the displacements and the drifts produced using the accelerograms corresponding to the Immediate Occupancy (IO) limit state are greater than the corresponding displacements and drifts calculated with the accelerograms used in ASCE. 41 to control the Collapse Prevention (CP) limit state.

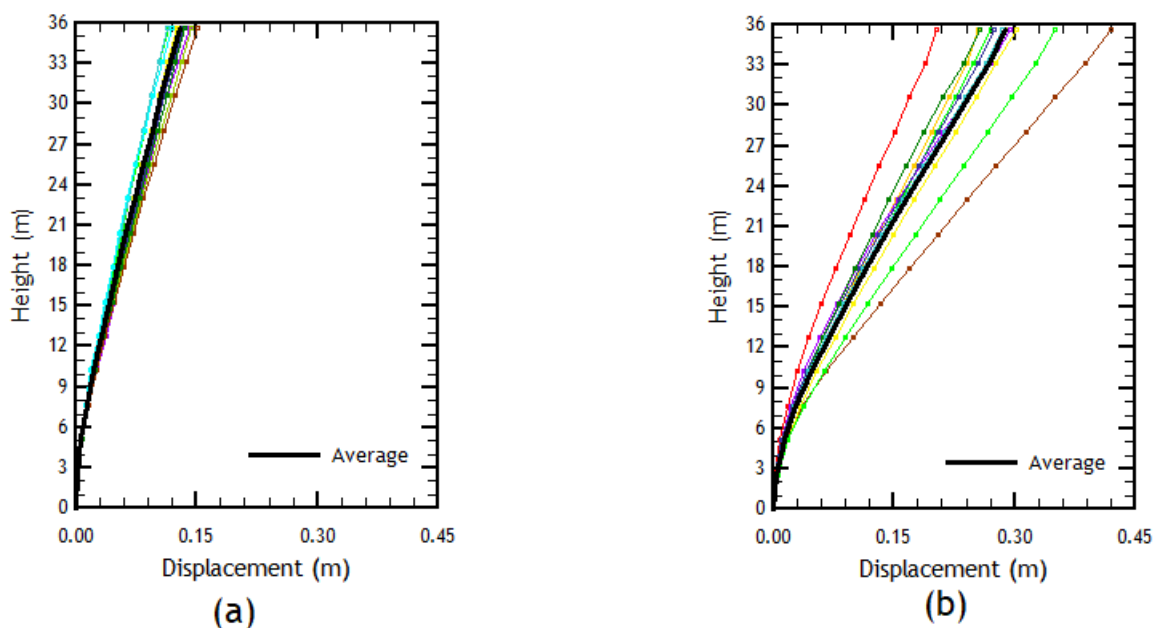


**Figure 12.** Floor displacements: (a) X direction; (b) Y direction. Immediate Occupancy Limit State.

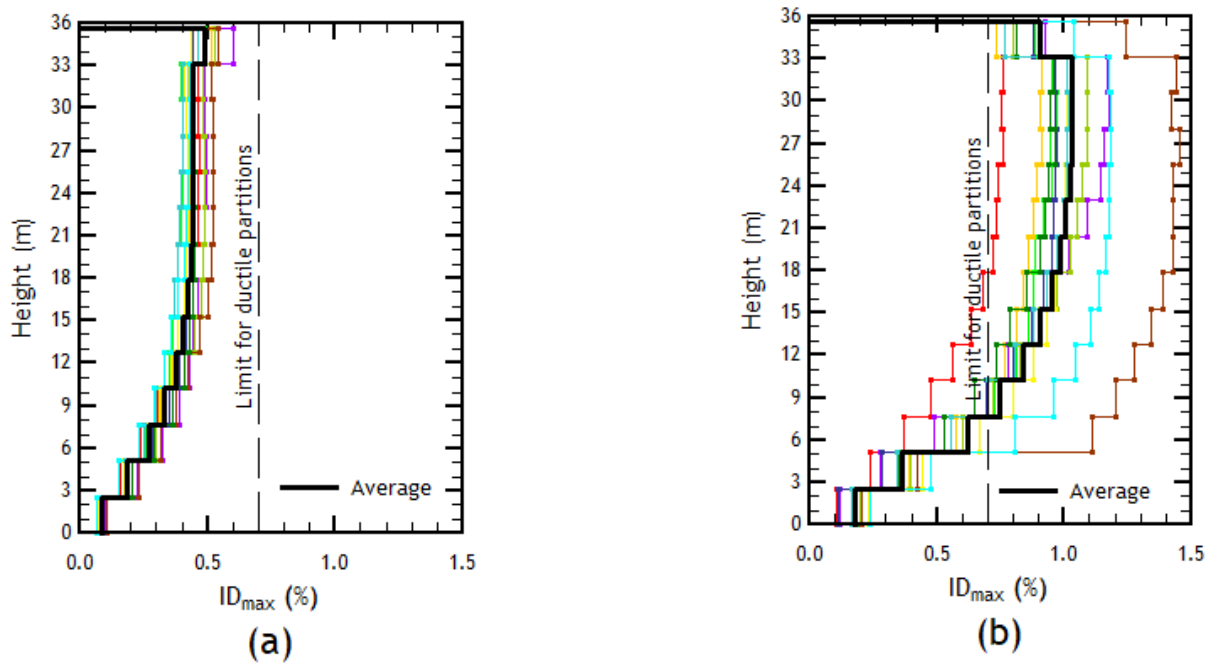


Figure 13. Story drifts: (a) X direction; (b) Y direction. Immediate Occupancy Limit State.

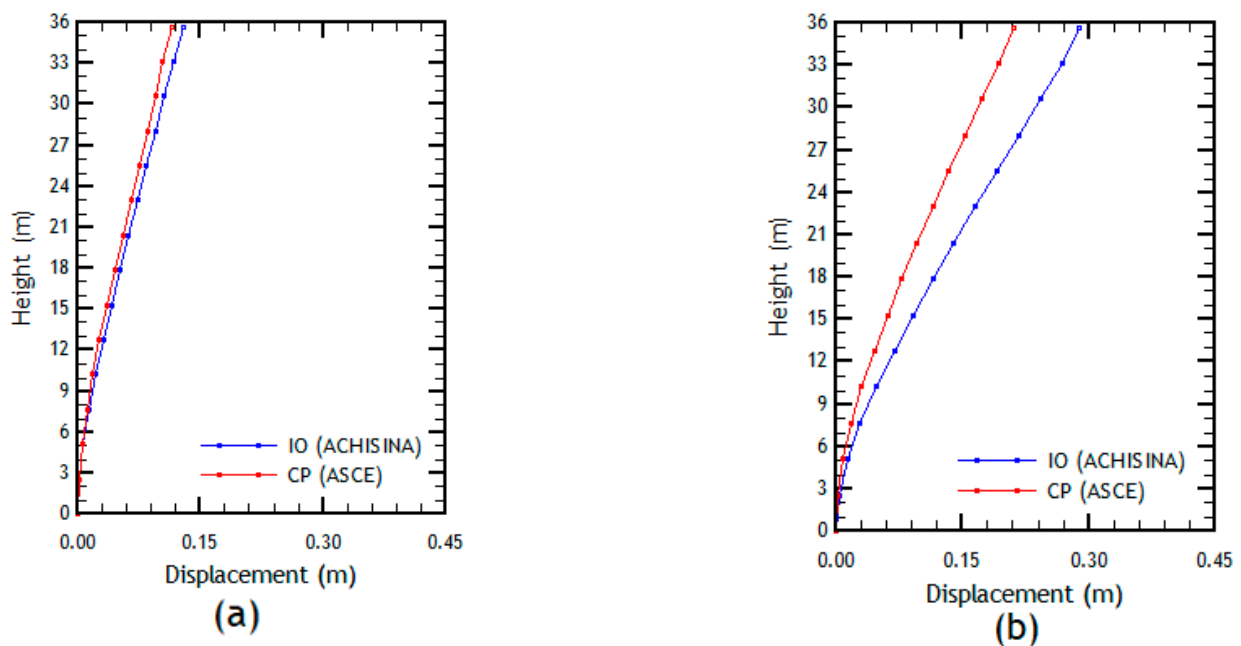
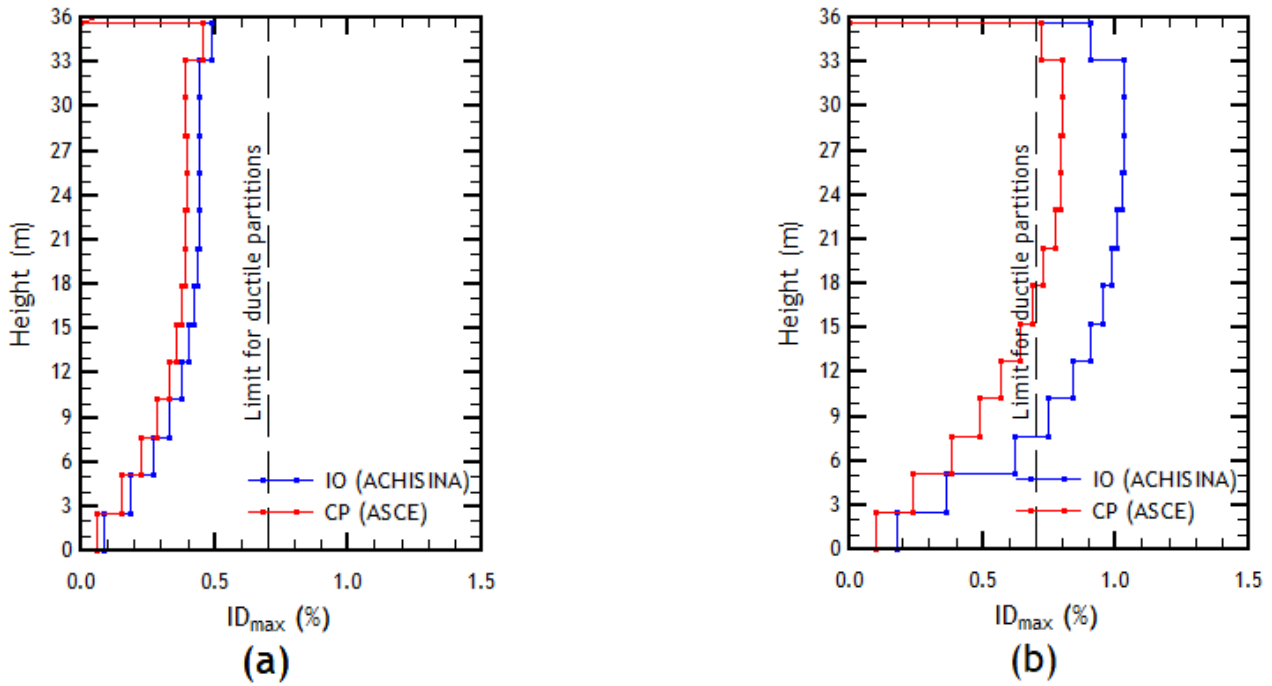


Figure 14. Comparison of displacements between ASCE 41-17 and ACHISINA analyses: (a) X direction; (b) Y direction.

It is possible to observe that, as for the nonlinear dynamic time history analysis performed by the ACHISINA methodology, it presents greater displacements than its counterpart in ASCE 41-17. This can be attributed to the difference between the seismic demands of both methods, with ACHISINA's demand being slightly higher in magnitude. However, the difference in the duration of the records used is more significant, as the Chilean records in Table 5 were used, unlike the artificial records generated with a duration of 10 s following the ASCE 41-17 method. In fact, there is a greater stiffness degradation for the first set of accelerograms due to the higher number of experienced cycles, with the greatest effect occurring in the Y direction as it moves further into the inelastic range of its elements.



**Figure 15.** Comparison of story drifts between ASCE 41-17 and ACHISINA analyses: (a) X direction; (b) Y direction.

To evaluate the local performance of the selected walls, Figures 16 and 17 show the comparison between the unit strains obtained for steel elongation and concrete shortening, as well as their respective acceptance criteria. It is worth noting that the wall in the Y direction has a confined edge element for the first two stories, so it would also be of interest to evaluate outside the confined element (referred to as the double mesh element) to determine if the selected confinement length is sufficient.

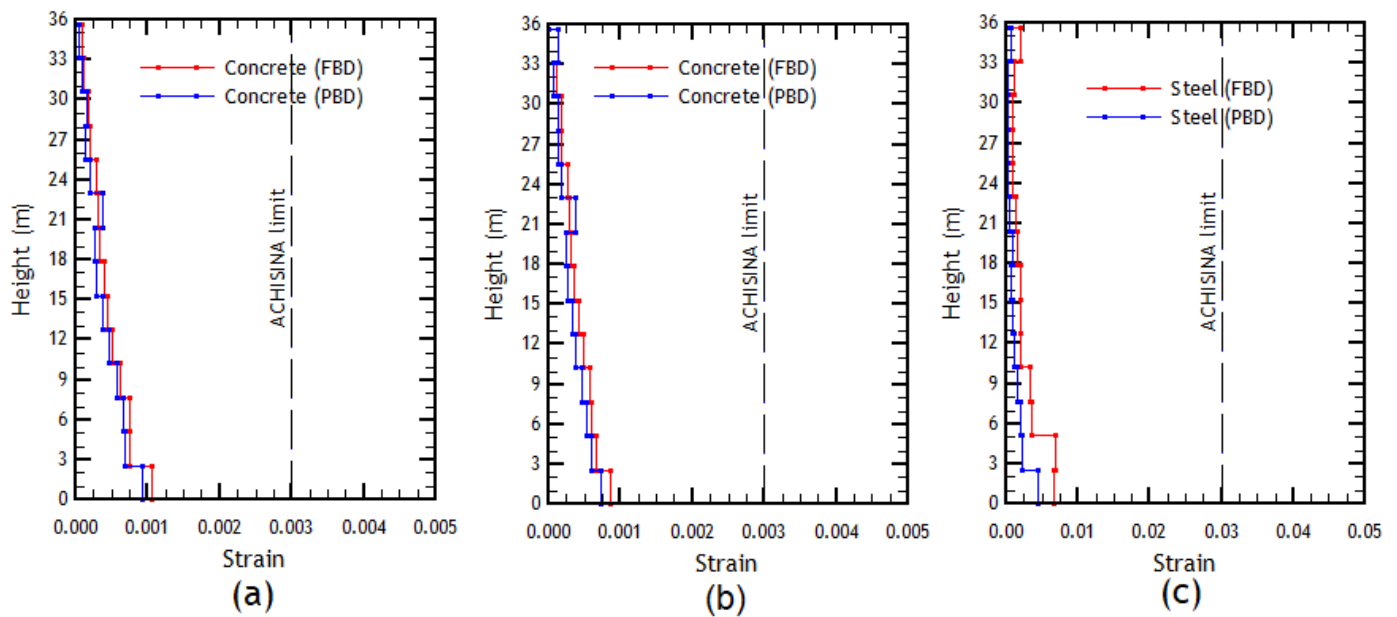


**Figure 16.** Unit strain comparison of the wall in the X direction and respective acceptance criteria under the FBD and PBD designs: (a) edge element concrete; (b) double mesh concrete; and (c) edge element reinforcing steel. Immediate Occupancy limit state.

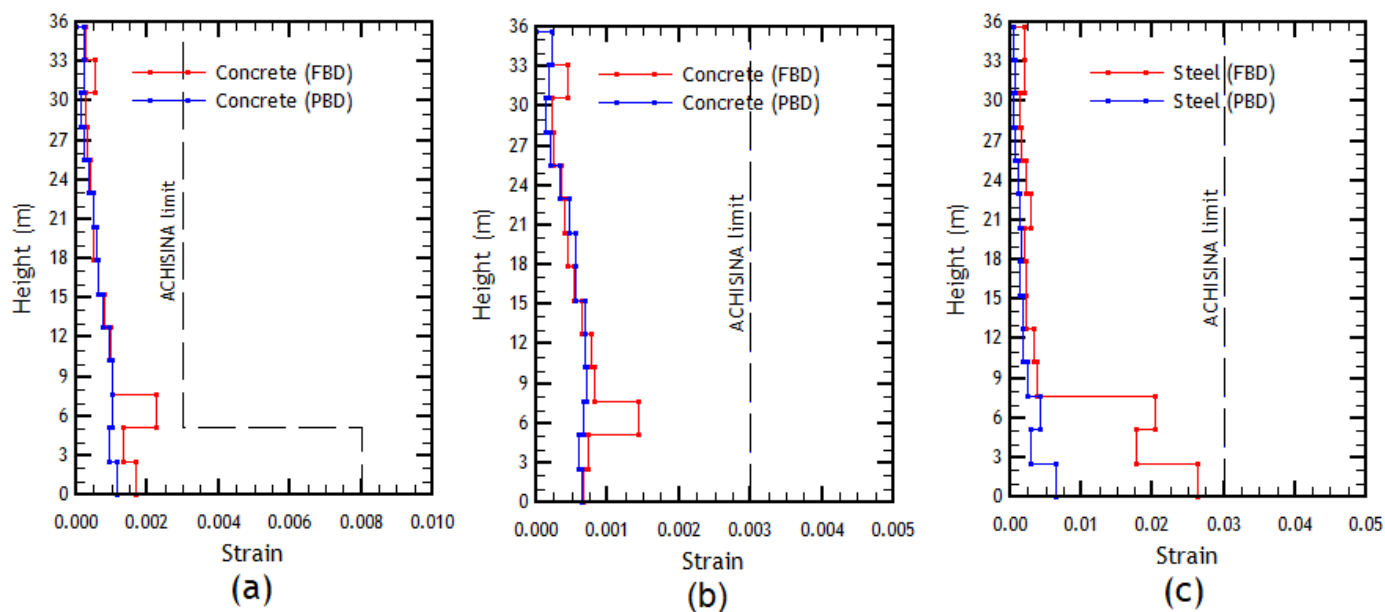


**Figure 17.** Unit strain comparison of the wall in the Y direction and respective acceptance criteria under the FBD and PBD designs: (a) edge element concrete; (b) double mesh concrete; and (c) edge element reinforcing steel. Immediate Occupancy limit state.

For the wall in the X direction, both the steel and concrete elements display a good response, with, by a considerable margin, none of the deformation limits being exceeded. Although the wall does not reach failure for this seismic demand, compression failure of concrete is expected to occur because it is closer to its limit, compared to the limit of steel. This is expected because it lacks edge elements with adequate confinement. Similarly, since there is no confinement, the comparison between the edge element and the double mesh is not relevant, and the demand-to-capacity ratio for the latter is always lower than that for the former.

For the shear wall selected in the Y direction, it can also be observed that none of the deformation limits imposed on the steel and concrete elements are exceeded. Compared to the shear wall in the X direction, the margins are smaller, approaching the limit for steel elongation on the first story, and, worryingly, the deformation limit for unconfined concrete on the third story, just outside the zone considered with special edge elements. This last point may be of great importance, because it presents an undesirable failure mode within the design reach, failing prematurely on the third story with little use of the additional deformation capacity that was engineered for the lower stories.

To have a complete picture of the shear wall response, it was decided to compare the imposed moment and shear demands with their expected capacity. For this, the capacity moment was determined as the value at which the shear wall is expected to yield considering the application of the axial force, according to the seismic weight of the building and the capacity at shear according to ACI318. Taking this into consideration, the average results are presented in Figures 18 and 19.

For the shear wall in the X direction, it can be noted that, as to the first level, it is very close to reaching the moment where plasticization can be expected to occur. This is a good indicator that the expected hinge formation mechanism in the critical section will develop. On the other hand, the demand for maximum shear stress does not exceed the capacity of the shear wall, indicating that the shear wall will primarily function in flexure.

Conversely, for the shear wall in the Y direction, it can be observed that as to the first and third levels, it is very close to reaching the moment where yielding can be expected to occur, possibly resulting in premature failure in the latter due to the lower capacity of the concrete, as observed in previous results. Additionally, the demand for shear stress also does not exceed the capacity of the shear wall, so flexural failure is expected.

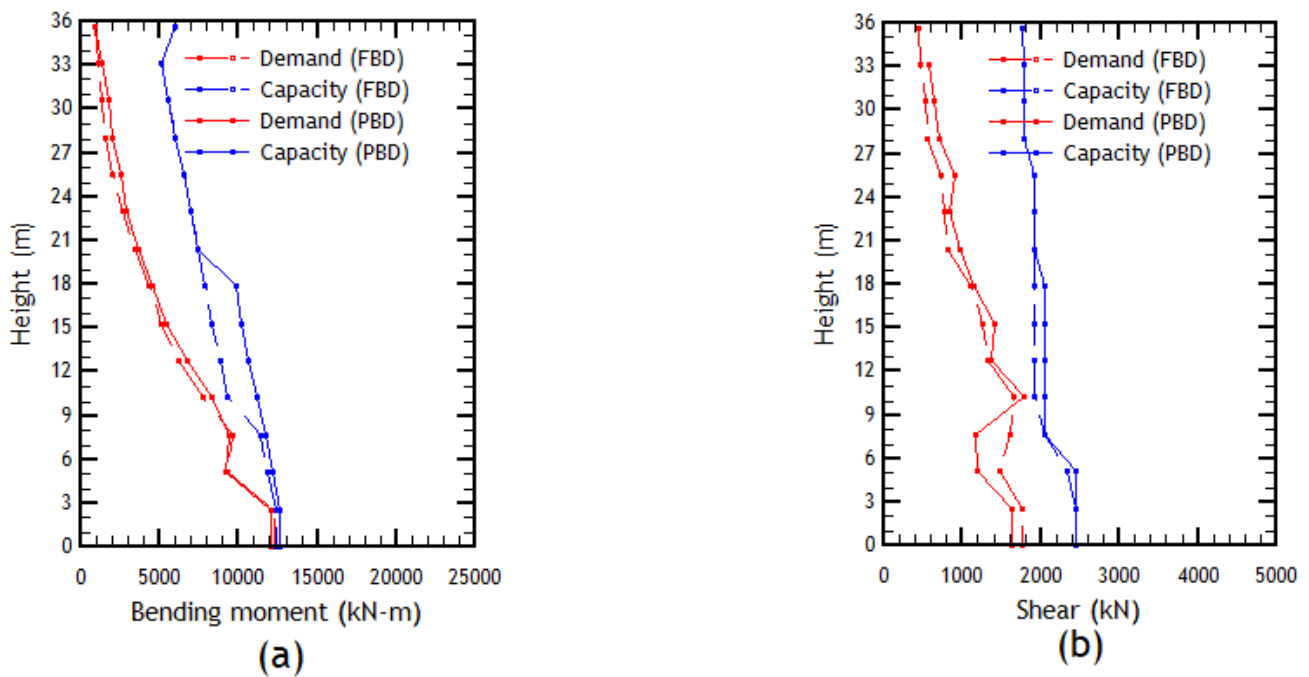


**Figure 18.** Comparison of the demand/capacity in the wall in the X direction under the FBD and PBD designs: (a) moment envelope; (b) shear envelope. Immediate Occupancy limit state.

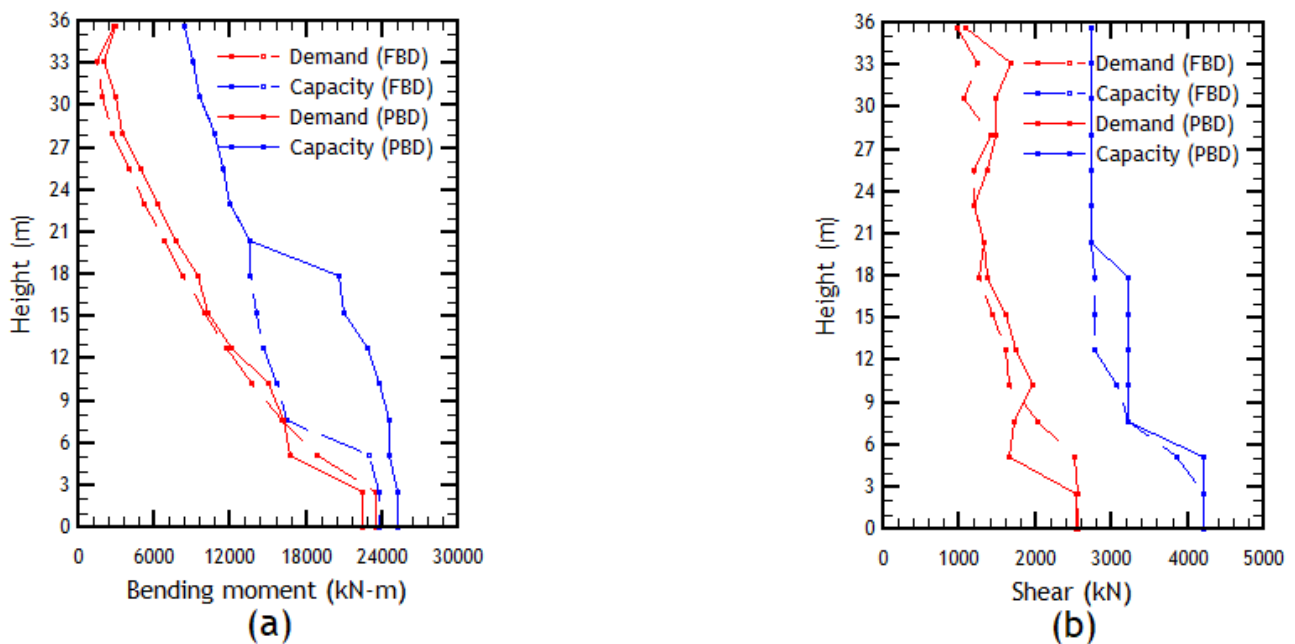


**Figure 19.** Comparison of the demand/capacity in the wall in the Y direction under the FBD and PBD designs: (a) moment envelope; (b) shear envelope. Immediate Occupancy limit state.

#### 4.2.2. Additional Deformation Capacity Limit State Results

The ultimate limit state corresponds only to the evaluation of local performance, where the same parameters as in the previous limit state are reviewed but while allowing for a greater range of damage for an amplified seismic demand, as stated in the methodology. Similarly, the comparison between the unit strains obtained for steel elongation and concrete shortening, together with their respective acceptance criteria, are shown in Figures 20 and 21.

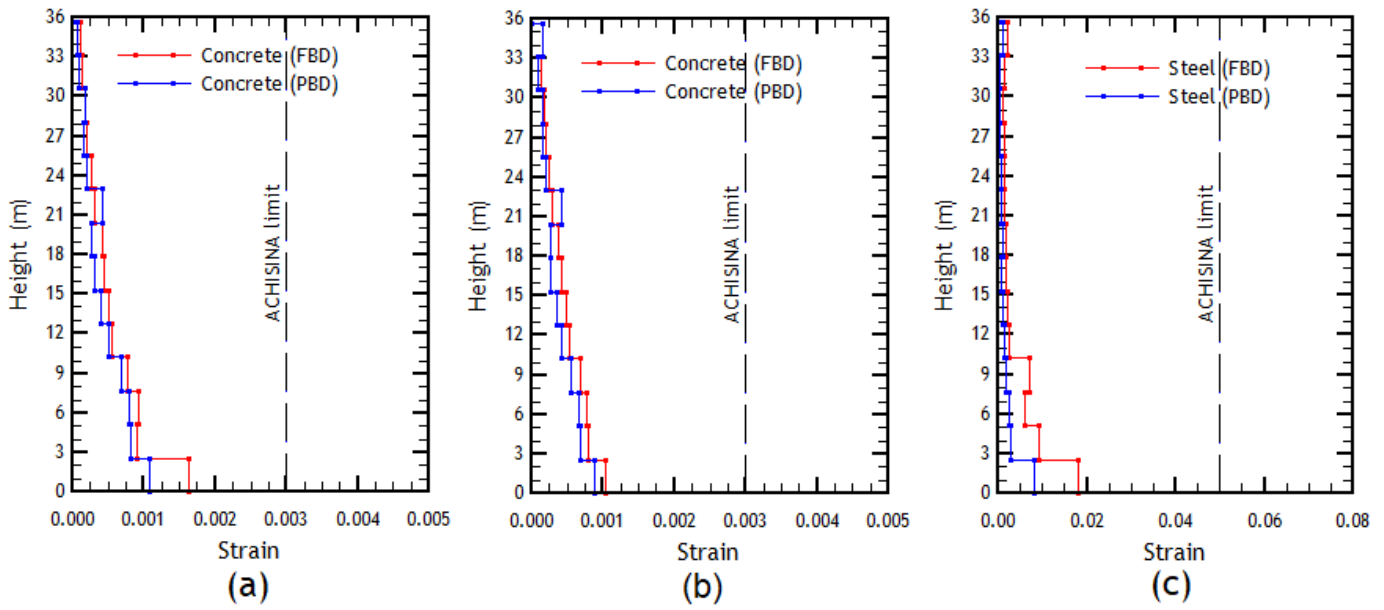


**Figure 20.** Unit strain comparison of the wall in the X direction and respective acceptance criteria under the FBD and PBD designs: (a) edge element concrete; (b) double mesh concrete; and (c) edge element reinforcing steel. Additional Deformation Capacity limit state.

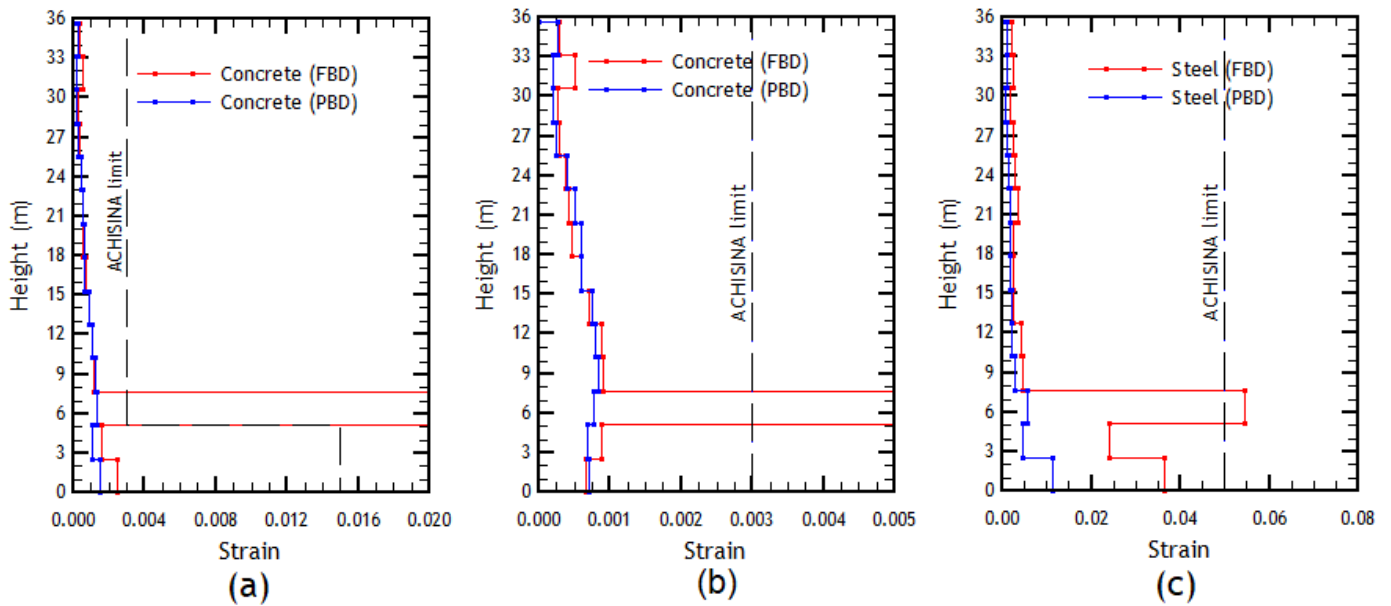


**Figure 21.** Unit strain comparison of the wall in the Y direction and respective acceptance criteria under the FBD and PBD designs: (a) edge element concrete; (b) double mesh concrete; and (c) edge element reinforcing steel. Additional Deformation Capacity limit state.

Regarding the shear wall in the X direction, a similar behavior to the previous limit state can be observed, with the deformation limits being met for both materials; although, with a higher demand/capacity ratio, this has more significance for concrete. This is not only because the seismic demand is considerably higher, but also that the limit for unconfined concrete has the same value of 0.003. On the other hand, there is still a higher demand located on the first story, so it is expected that failure will occur at this level, fulfilling the definition of the critical section made in the design stage. Similarly, since it does not have confinement, it is not important to study the deformations that occurred outside of the special boundary elements.

The wall in the Y direction reveals that, on the third story, both materials exceed their limits, presenting considerable deformation values compared to the capacity of the concrete. These results can be attributed to the loss of the bending resistance capacity, considering the significant reductions in steel reinforcement, thickness, and grade of concrete used between the first two stories and the upper stories. In fact, instead of concentrating plastic deformations in the first stories, they are occurring on the third story, the design of which is not properly engineered to handle large deformations.

To validate these assumptions, the imposed demands of moment and shear are compared to their expected capacity in the same manner as when performed for the previous limit state. The results of this comparison are shown in Figures 22 and 23 for the wall in the X and Y directions, respectively.

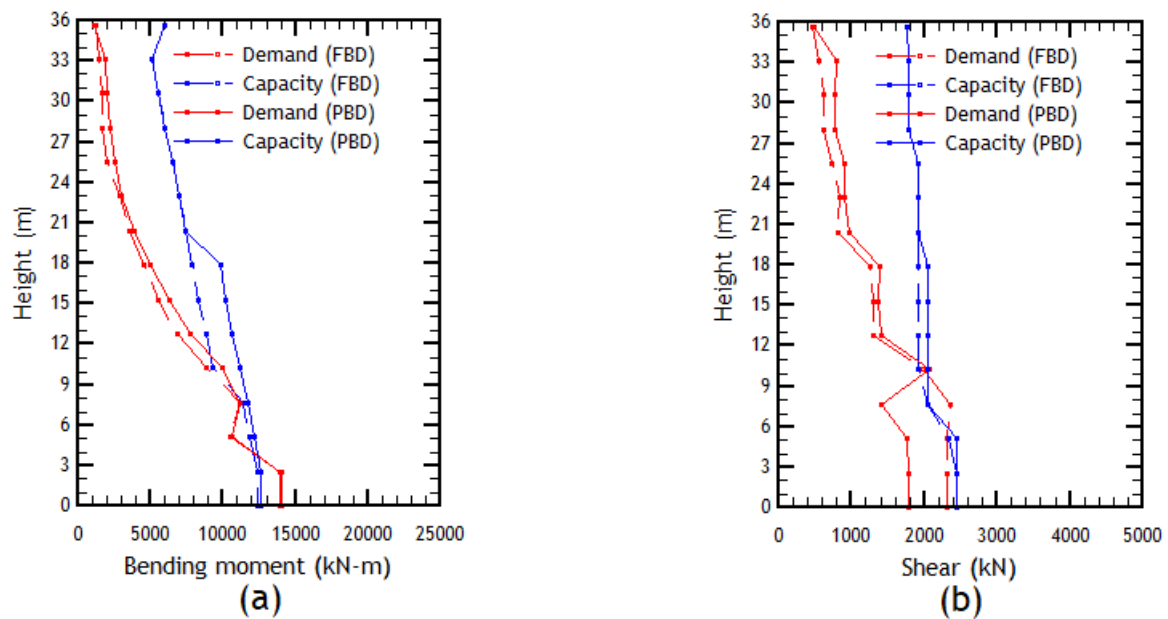


**Figure 22.** Comparison of the demand/capacity in the wall in the X direction under the FBD and PBD designs: (a) moment envelope; (b) shear envelope. Additional Deformation Capacity limit state.

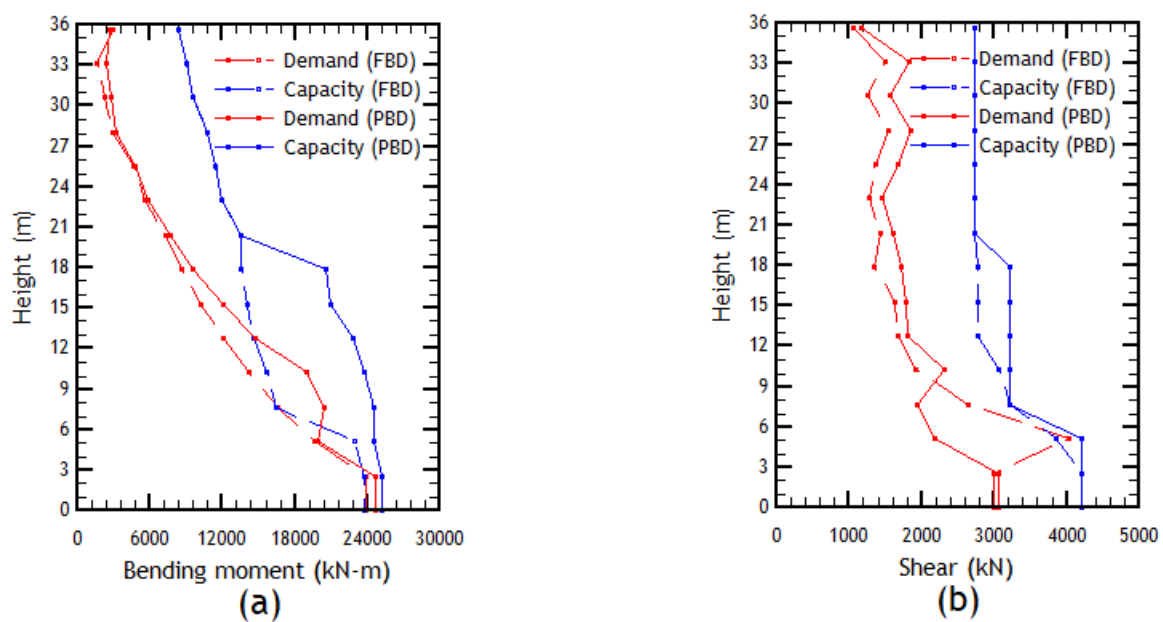


**Figure 23.** Comparison of the demand/capacity in the wall in the Y direction under the FBD and PBD designs: (a) moment envelope; (b) shear envelope. Additional Deformation Capacity limit state.

The wall in the X direction shows that, for the first story, the moment value where yielding occurs is exceeded, fulfilling the assumption of the critical section in this story. However, for stories three and four, the limits of shear stress resistance are exceeded, producing a shear failure prior to the complete development of the failure due to yielding. This may be due to the underestimation of the contribution of the upper modes to the shear envelope and the failure to consider the lower stories corresponding to the underground levels within the model.

The analysis of the wall in the Y direction shows that the yield moment is reached on the first and third stories, which confirms the previous results regarding the displacements achieved on the roof. In fact, it is possible for the shear wall to undergo plastic deformation at both stories, with most of the rotation occurring at the third story rather than the first, which was not intended in the original capacity design performed using the linear procedure.

On the other hand, it was found that the shear stress limit is exceeded at the second story, although this occurs after the failure of the concrete fiber under compression, which is relevant for studying the possible failure mechanism of this element.

#### 4.2.3. PBD Compliant Redesign

Based on the results obtained in Sections 4.2.1 and 4.2.2 and following the recommended procedure of ACHISINA [11], it is evident that the limits established for interstory drift and deformations for the Serviceability and Additional Deformation limit states, respectively, are not met. Therefore, in the following section, this paper seeks to evaluate the building and redesign it to meet these acceptance criteria. After applying the PBD, the dynamic characteristics of the building have been modified, and this affects the results. To apply the nonlinear analysis again, the same accelerograms used for the analysis of the building obtained with the FBD are used, since these have been paired for a range of periods between 0.05 s and 4.00 s., within which the new predominant periods in each direction of analysis are included.

Regarding the global behavior observed at the Serviceability limit state, as shown in Figure 15 for the analysis conducted in the Y direction, it can be extrapolated that it is necessary to stiffen the involved walls by using higher-strength concrete or increasing their thicknesses. Conversely, it is not necessary to apply these changes to the walls acting in the X direction, as their larger dimensions and the concentration of walls acting in this direction are sufficient to comply with the limits established in the procedure.

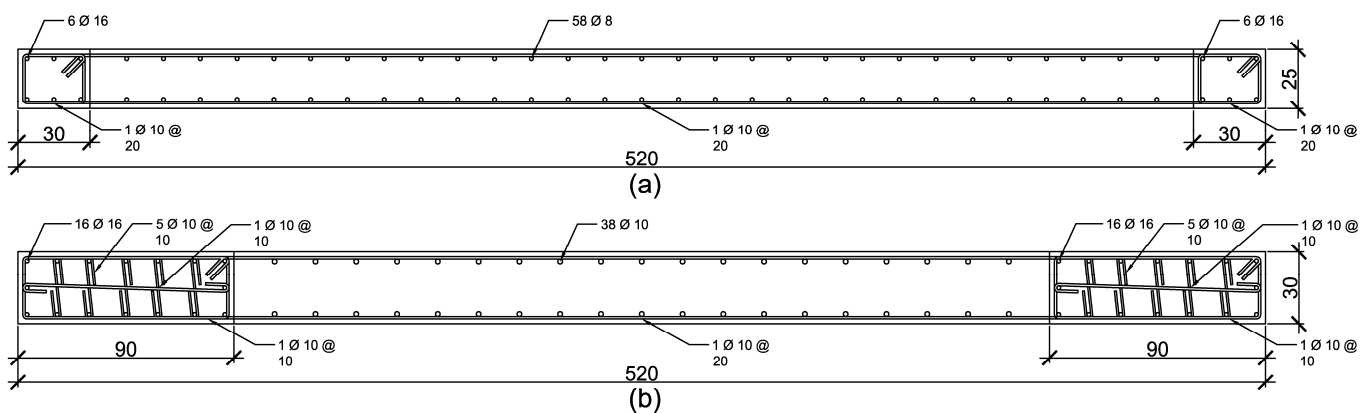
Additionally, as mentioned in Figures 21 and 23, it is necessary to ensure that the concentration of deformations occurs in the critical section defined in the original design. To achieve this, the walls should be redesigned by gradually transitioning the flexural resistance moment along their height, increasing the thickness and utilizing higher strength concrete in the concrete walls, and enhancing their reinforcement detailing.

Based on the previous criteria, the building is thereby redesigned to meet the acceptance criteria that were previously not met with the original design. To illustrate these changes, Table 9 shows the changes in wall thickness and concrete strength for each story, and Figure 24 shows an example of the modified reinforcement detail of a shear wall. It should be noted that changes regarding steel reinforcement only apply to half of the full height of the shear walls, as this was where the greatest deficiency in necessary resistance capacity was observed.

Figures 16 and 17 display the results of the unit strain comparison for element deformation, and Figures 18 and 19 the moment and shear demand versus capacity for the Serviceability limit state. For the Additional Deformation limit state, the unit strain comparison for element deformation is shown in Figures 20 and 21, and for the moment and shear demand versus capacity in Figures 22 and 23.

**Table 9.** Comparison of the concrete grades and wall thicknesses between the original design and redesign.

Story	FBD			PBD		
	Concrete (MPa)	Width X (cm)	Width Y (cm)	Concrete (MPa)	Width X (cm)	Width Y (cm)
8 to 14	25	20	20	35	20	25
7	25	20	20	35	20	30
6	30	20	20	35	20	30
5	30	20	20	35	20	30
4	30	20	25	35	20	30
3	35	20	25	35	20	30
2	35	20	30	35	20	30
1	35	20	30	35	20	30

**Figure 24.** Comparative example of the structural detail of (a) the wall obtained using FBD and (b) the wall obtained using PBD.

Regarding the obtained figures, it is evident that for the X direction, a similar behavior to that exhibited by applying the FBD is maintained, mainly because there have been no substantial changes in the dimensions or arrangement of the steel reinforcement for both limit states. However, for the Y direction in the Serviceability limit state, it can be observed that the third-floor wall does not show higher magnitudes of deformations, as observed in the original design. Similarly, the comparison between moment demand and capacity seems to indicate the formation of the critical section on the first floor. Conversely, for the Additional Deformation limit state, a substantial improvement in incurred deformations is presented, meeting the specified requirements for concrete material. In fact, the comparison between demand and capacity for flexural moment indicates that, when utilizing PBD, the resulting structure managed to rectify the deficiencies presented by the original design on floors 3–7, allowing for the development of the plastic hinge within the critical section as defined in the design stage.

The comparison of the interstory drifts and maximum displacement incurred in the original design and the redesign are shown in Figures 25 and 26, respectively. For the measurements taken in the X direction, a slight increase is observed in the maximum incurred displacement, which can be attributed to an increase in flexibility due to the total mass of the building having increased without a corresponding increase in stiffness compared to the previous model. With respect to the Y direction, a substantial improvement in behavior can be observed, with a general reduction of up to 30% in the maximum displacement, surpassing the limit of ductile partitions up to a maximum of 0.05% on the upper floors.

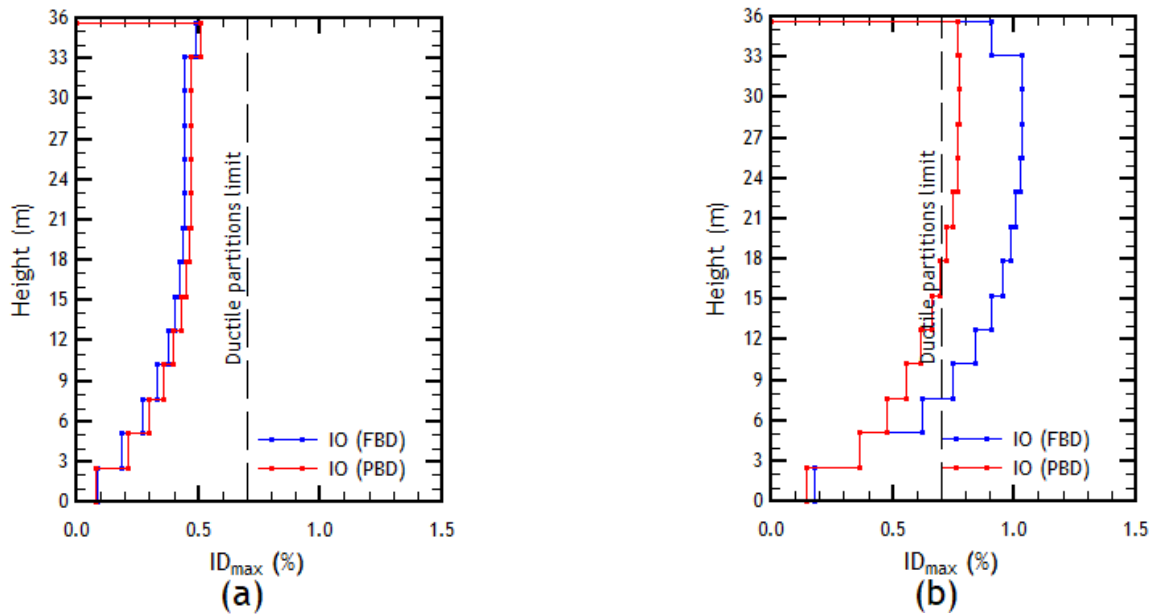


**Figure 25.** Comparison of interstory drifts, building under FBD and PBD design: (a) X direction; (b) Y direction.

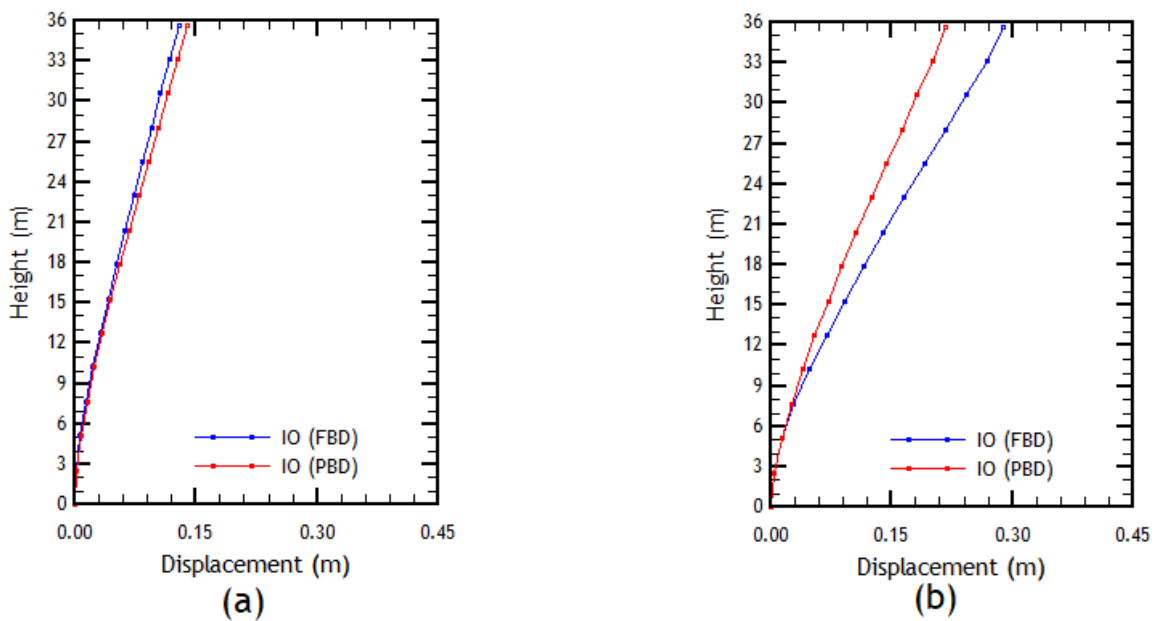


**Figure 26.** Comparison of displacements under the FBD and PBD designs: (a) X direction; (b) Y direction.

It can be concluded that the structure obtained with PBD was able to overcome the deficiencies presented in the structure obtained with FBD according to the performance-based analysis results. Strictly speaking, it is necessary to increase the stiffness in the Y direction to fully comply with the interstory drift limit for the Serviceability limit state. However, an important aspect to consider is the increase in costs which would be involved in opting for a project that meets the acceptance criteria indicated in the ACHISINA alternative procedure [51]. Based on this, a comparison of material volumes and weights is presented in Table 10, using the actual volume of the FBD structure and an approximate estimation for the PBD structure. The increase in the quantity of materials achieved by applying PBD in accordance with Chilean provisions is in line with the findings of a

previous study [66], in which the cost difference between FBD and PBD amounted to only 2% of the cost of the superstructure of the building.

**Table 10.** Comparison of material quantity between structures obtained according to FBD and PBD.

	Concrete Volume (m <sup>3</sup> )	Steel Weight (kg)
FBD	3329.44	338,271.91
PBD	3404.31	357,864.31
Difference	+2.25%	+5.79%

## 5. Conclusions

In this work, performance-based design utilized in Chile has been applied to a residential building and compared with conventional force-based design, and both were then in turn compared with the application of American performance-based design standards.

The pushover analysis of the structure obtained using force-based design (FBD) provides information on the expected behavior of the structure through the capacity curve, where it is evident that the Y direction is more flexible than the X direction, reaching plastic deformation with a roof displacement of 6 cm. This indicates that greater stiffness is necessary, as evidenced by noncompliance with the floor drift limits according to the ACHISINA limits, in contrast to the X direction, which is located at a point where large deformations are not incurred, which therefore meets the requirement. These results show a lack of consensus between the Chilean FBD codes and the ACHISINA procedure, in which the latter has a more stringent requirement for the drift limits. Thus, it is required to reevaluate these limits to fulfill the scope of the PBD methodology, in which a design can be validated when it is deemed noncompliant with FBD requirements. Nevertheless, these aspects have been considered in the structure obtained by applying performance-based design (PBD).

On the other hand, the performance points determined according to ASCE 41-17 require further study. Although a good fit was presented in the X direction for the Collapse Prevention performance level according to this standard, it was exceeded considerably in the Y direction. This appears to indicate a limitation in the ASCE 41-17 target displacement determination approach for the pushover analysis, as compared to the TH analysis, specifically for flexible structures. Further studies must be conducted to evaluate the coefficients used for the target displacement for buildings with higher primordial periods in which the inelastic and cyclic behavior are not simplified to a set value in the code.

Regarding nonlinear dynamic time history analyses, the agreeable performance of the structure can be emphasized using the procedure executed according to ASCE 41-17 and ASCE 7-16 standards, being only exceeded in deformation limits in the Immediate Occupancy (IO) limit state for the wall in the X direction. On the other hand, the overall structural performance was evaluated using the limits established by ASCE 7-16 and LATBSDC standards and met these standards with a considerable margin of safety. The reason for this behavior was determined to be the limits of the methodology, which is primarily focused on frame structures typical of the United States.

Through the analysis by the ACHISINA method, it can be concluded that, although the structure obtained by FBD meets the established criteria for the limit state of IO, it was necessary to review the design of the wall elements, especially those corresponding to the Y direction. In fact, there is a clear need to maintain moment capacity over height to avoid the formation of plastic hinges outside the critical zone defined in the design stage, resulting in the underutilization of the increased deformation capacity of the confined edge elements belonging to the first two stories. Therefore, it might be necessary to include in the FBD procedure requirements that account for the participation of higher modes in the design. For this, it is recommended that designs avoid abrupt changes in wall thickness, material grades, and reinforcement disposition in the design, all of which occur notably in this case study, considering the occurrence of higher moments at intermediate levels due to the greater participation of higher modes.

When comparing the methodologies applied in the design of a building (FBD and PBD), differences in their application and in the resulting measured data are evident, with the difference between the applied seismic records being critical. Additionally, it is suggested that the matching of accelerograms to be used in the analyses for assessing the performance of structures be included, whether they are recorded or artificial accelerograms, using the complete range of periods relevant to the structural response, instead of relying solely on the recommendation to match between 0.5 T and 1.25 T. Another point of consideration is the duration of the records, where there are significant variations in roof displacements between the two applied analyses, being greater when complete Chilean records were used instead of artificial accelerograms. This highlights the importance of coherent methodology selection based on the conditions of the study area.

Additionally, it is necessary to investigate beam acceptance criteria, considerations which were not thoroughly addressed in this report; studying the way the criteria are evaluated in the ACHISINA method, specifically, defining a limit of plastic deformation in the IO limit state, and no limit regarding the evaluation of Additional Deformation capacity. Additional acceptance criteria are deemed required.

The increase in the quantity of materials when applying the PBD is 2.25% for concrete, and 5.50% for reinforcing steel, compared to the FBD. This increase is consistent with the cost variation reported in a study conducted that applied American design standards [2]. Further study can be taken up to evaluate the PBD enhancement on the buildings' performance during their lifespan by conducting a fragility study to determine the impact of design types on the performance of different components, under the application of the FEMA P-58 methodology [31].

Furthermore, it is recommended that future studies consider the procedures derived from the use of performance-based design with European standards, in order to further enrich the discussion introduced in this study.

**Author Contributions:** Conceptualization, J.C.V. and J.C.; methodology, J.C.V. and J.C.V.-Q.; software, J.C.V.-Q.; validation, J.C.V.-Q., J.C.V. and J.C.; formal analysis, J.C.V.-Q.; investigation, J.C.V.-Q.; resources, J.C.V.-Q.; data curation, J.C.V. and J.C.; writing—original draft preparation, J.C.V.-Q.; writing—review and editing, J.C.V.; visualization, J.C.; supervision, J.C.V. and J.C. All authors have read and agreed to the published version of the manuscript.

**Funding:** This research was funded by Agencia Nacional de Investigación y Desarrollo (ANID Chile), grant number FOVI 210063.

**Data Availability Statement:** The relevant data from this research are available in the authors' repositories.

**Acknowledgments:** The authors thank the Pontificia Universidad Católica de Valparaíso for the support provided in the development of the research, as well as the support in the publication of the article. The authors acknowledge access to strong-motion data through the Center for Engineering Strong Motion Data (CESMD), last visited on 22 January 2022. The networks or agencies providing the data used in this report are the California Strong Motion Instrumentation Program (CSMIP) and the USGS National Strong Motion Project (NSMP).

**Conflicts of Interest:** The authors declare no conflict of interest.

## References

1. Moehle, J.P. Nonlinear analysis for performance-based earthquake engineering. *Struct. Des. Tall Spec. Build.* **2005**, *14*, 385–400. [[CrossRef](#)]
2. Yang, T.Y.; Moehle, J.P.; Bozorgnia, Y.; Zareian, F.; Wallace, J.W. Performance assessment of tall concrete core-wall building designed using two alternative approaches: Performance assessment of tall concrete core wall buildings. *Earthq. Eng. Struct. Dyn.* **2012**, *41*, 1515–1531. [[CrossRef](#)]
3. Klemencic, R.; Fry, J.A.; Hooper, J.D. Performance-based design of tall reinforced concrete ductile core wall systems. *Struct. Des. Tall Spec. Build.* **2006**, *15*, 571–579. [[CrossRef](#)]
4. Aly, N.; Galal, K. Seismic performance and height limits of ductile reinforced masonry shear wall buildings with boundary elements. *Eng. Struct.* **2019**, *190*, 171–188. [[CrossRef](#)]

5. Jeon, S.-H.; Park, J.-H. Seismic Fragility of Ordinary Reinforced Concrete Shear Walls with Coupling Beams Designed Using a Performance-Based Procedure. *Appl. Sci.* **2020**, *10*, 4075. [[CrossRef](#)]
6. Dabaghi, M.; Saad, G.; Allhassania, N. Seismic Collapse Fragility Analysis of Reinforced Concrete Shear Wall Buildings. *Earthq. Spectra* **2019**, *35*, 383–404. [[CrossRef](#)]
7. Abdullah, S.A.; Wallace, W. Reliability-Based Design Methodology for Reinforced Concrete Structural Walls with Special Boundary Elements. *ACI Struct. J.* **2020**, *117*, 3. [[CrossRef](#)]
8. Kolozvari, K.; Terzic, V.; Miller, R.; Saldana, D. Assessment of dynamic behavior and seismic performance of a high-rise rc coupled wall building. *Eng. Struct.* **2018**, *176*, 606–620. [[CrossRef](#)]
9. Arifin, F.A.; Sullivan, T.J.; MacRae, G.; Kurata, M.; Takeda, T. Lessons for loss assessment from the Canterbury earthquakes: A 22-story building. *Bull. Earthq. Eng.* **2021**, *19*, 2081–2104. [[CrossRef](#)]
10. Ji, X.; Liu, D.; Molina Hutt, C. Seismic performance evaluation of a high-rise building with novel hybrid coupled walls. *Eng. Struct.* **2018**, *169*, 216–225. [[CrossRef](#)]
11. Tojo, T.; Tanaka, K.; Yamamoto, S.; Tsunashima, N.; Suzuki, T.; Takada, A.; Yabushita, N. Evaluation of seismic performance for the complex structure of planar arrangement with reinforced concrete shear walls. *AIJ J. Technol. Des.* **2020**, *26*, 91–96. [[CrossRef](#)]
12. Zhong, K.; Lin, T.; Deierlein, G.G.; Graves, R.W.; Silva, F.; Luco, N. Tall building performance-based seismic design using SCEC broadband platform site-specific ground motion simulations. *Earthq. Eng. Struct. Dyn.* **2021**, *50*, 81–98. [[CrossRef](#)]
13. Vielma, J.C.; Barbat, A.H.; y Oller, S. Seismic safety of low ductility structures used in Spain. *Bull. Earthq. Eng.* **2010**, *8*, 135–155. [[CrossRef](#)]
14. Hagen, G.R. Performance-Based Analysis of a Reinforced Concrete Shear Wall Building. Master's Thesis, California Polytechnic State University, San Luis Obispo, CA, USA, 2012. [[CrossRef](#)]
15. Pozo, J.D.; Hube, M.A.; Kurama, Y.C. Quantitative assessment of nonlinear macromodels for global behavior and design of planar RC walls. *Eng. Struct.* **2020**, *224*, 111190. [[CrossRef](#)]
16. Chan-Anan, W.; Leelataviwat, S.; Goel, S.C. Performance-based plastic design method for tall hybrid coupled walls: Performance-Based Plastic Design Method. *Struct. Des. Tall Spec. Build.* **2016**, *25*, 681–699. [[CrossRef](#)]
17. Klemencic, R.; Fry, J.A.; Hooper, J.D.; Morgen, B.G. Performance-based design of ductile concrete core wall buildings—Issues to consider before detailed analysis. *Struct. Des. Tall Spec. Build.* **2007**, *16*, 599–614. [[CrossRef](#)]
18. Zeris, C.; Lalas, A.; Spacone, E. Performance of torsionally eccentric RC wall frame buildings designed to DDBD under bidirectional seismic excitation. *Bull. Earthq. Eng.* **2020**, *18*, 3137–3165. [[CrossRef](#)]
19. O'Reilly, G.J.; Calvi, G.M. Conceptual seismic design in performance-based earthquake engineering. *Earthq. Eng. Struct. Dyn.* **2019**, *48*, 389–411. [[CrossRef](#)]
20. Sommer, A.; Bachmann, H. Seismic behavior of asymmetric RC wall buildings: Principles and new deformation-based design method. *Earthq. Eng. Struct. Dyn.* **2005**, *34*, 101–124. [[CrossRef](#)]
21. Zhai, Z.; Guo, W.; Li, Y.; Yu, Z.; Cao, H.; Bu, D. An improved performance-based plastic design method for seismic resilient fused high-rise buildings. *Eng. Struct.* **2019**, *199*, 109650. [[CrossRef](#)]
22. Alarcón, C.; López, A.; Vielma, J.C. Performance of Medium-Rise Buildings with Reinforced Concrete Shear Walls Designed for High Seismic Hazard. *Materials* **2023**, *16*, 1859. [[CrossRef](#)] [[PubMed](#)]
23. Carrillo, J.; Alcocer, S.M. Acceptance limits for performance-based seismic design of RC walls for low-rise housing: Acceptance limits for pbsd of rc walls for low-rise housing. *Earthq. Eng. Struct. Dyn.* **2012**, *41*, 2273–2288. [[CrossRef](#)]
24. Terzic, V.; Kolozvari, K.; Saldana, D. Implications of modeling approaches on seismic performance of low- and mid-rise office and hospital shear wall buildings. *Eng. Struct.* **2019**, *189*, 129–146. [[CrossRef](#)]
25. Fragiadakis, M.; Papadrakakis, M. Performance-based optimum seismic design of reinforced concrete structures. *Earthq. Eng. Struct. Dyn.* **2008**, *37*, 825–844. [[CrossRef](#)]
26. Georgoussis, G.K. Yield Displacements of Wall-Frame Concrete Structures and Seismic Design Based on Code Performance Objectives. *J. Earthq. Eng.* **2021**, *25*, 566–578. [[CrossRef](#)]
27. ASCE. *Minimum Design Loads and Associated Criteria for Buildings and Other Structures*; ASCE/SEI 7-16; American Society of Civil Engineers: Reston, Virginia, 2017.
28. ASCE. *Seismic Evaluation and Retrofit of Existing Buildings*; ASCE/SEI 41-17; American Society of Civil Engineers: Reston, Virginia, 2017.
29. PEER. *Guidelines for Performance-Based Seismic Design of Tall Buildings*; TBI; Pacific Earthquake Engineering Research Center, College of Engineering, University of California: Berkeley, CA, USA, 2017.
30. LATBSDC. *An Alternative Procedure for Seismic Analysis and Design of Tall Buildings Located in the Los Angeles Region*; Tall Buildings Structural Design Council: Los Angeles, CA, USA, 2020.
31. FEMA. *Guidelines for Performance-Based Seismic Design of Buildings, P-58-6*; Applied Technology Council for the Federal Emergency Management Agency: Washington, DC, USA, 2018.
32. Haselton, C.B.; Baker, J.W.; Stewart, J.P.; Whittaker, A.S.; Luco, N.; Fry, A.; Hamburger, R.O.; Zimmerman, R.B.; Hooper, J.D.; Charney, F.A. Response History Analysis for the Design of New Buildings in the NEHRP Provisions and ASCE/SEI 7 Standard: Part I—Overview and Specification of Ground Motions. *Earthq. Spectra* **2017**, *33*, 373–395. [[CrossRef](#)]
33. Haselton, C.B.; Fry, A.; Hamburger, R.O.; Baker, J.W.; Zimmerman, R.B.; Luco, N.; Elwood, K.J.; Hooper, J.D.; Charney, F.A.; Pekelnicky, R.G. Response History Analysis for the Design of New Buildings in the NEHRP Provisions and ASCE/SEI 7 Standard: Part II—Structural Analysis Procedures and Acceptance Criteria. *Earthq. Spectra* **2017**, *33*, 397–417. [[CrossRef](#)]

34. Sattar, S.; Hulsey, A.; Hagen, G.; Naeim, F.; McCabe, S. Implementing the performance-based seismic design for new reinforced concrete structures: Comparison among ASCE/SEI 41, TBI, and LATBSDC. *Earthq. Spectra* **2021**, *37*, 2150–2173. [[CrossRef](#)]
35. Buniya, M.K.; Barbosa, A.R.; Sattar, S. Assessment of a 12-Story Reinforced Concrete Special Moment Frame Building Using Performance-Based Seismic Engineering Standards and Guidelines: ASCE 41, TBI, and LATBSDC. *Ac. Struct. J.* **2020**. Available online: [https://tsapps.nist.gov/publication/get\\_pdf.cfm?pub\\_id=923632](https://tsapps.nist.gov/publication/get_pdf.cfm?pub_id=923632) (accessed on 2 March 2022).
36. Tafraout, S.; Bourahla, N.; Bourahla, Y.; Mebarki, A. Automatic structural design of RC wall-slab buildings using a genetic algorithm with application in BIM environment. *Autom. Constr.* **2019**, *106*, 102901. [[CrossRef](#)]
37. Zou, X.-K.; Chan, C.-M. Optimal seismic performance-based design of reinforced concrete buildings using nonlinear pushover analysis. *Eng. Struct.* **2005**, *27*, 1289–1302. [[CrossRef](#)]
38. EN 1998-3 (2005); Eurocode 8: Design of Structures for Earthquake Resistance. CEN: Brussels, Belgium, 2004.
39. Bommer, J.; Pinho, R. Adapting earthquake actions in Eurocode 8 for performance-based seismic design. *Earthq. Eng. Struct. Dyn.* **2006**, *35*, 39–55. [[CrossRef](#)]
40. Muho, E.; Papagiannopoulos, G.; Beskos, D. Deformation dependent equivalent modal damping ratios for the performance-based seismic design of plane R/C structures. *Soil Dyn. Earthq. Eng.* **2020**, *129*, 105345. [[CrossRef](#)]
41. Falcão Moreira, R.; Varum, H.; Castro, J.M. On the Applicability of Conventional Seismic Design Methodologies to Hybrid RC-Steel Systems. *Buildings* **2022**, *12*, 1558. [[CrossRef](#)]
42. Aydemir, C.; Eser, M.; Arslan, G. Drift capacity and allowable axial load level of RC columns. *Structures* **2023**, *48*, 1072–1081. [[CrossRef](#)]
43. Vamvatsikos, D.; Bakalis, K.; Kohrangi, M.; Pyrza, S.; Castiglioni, C.A.; Kanyilmaz, A.; Morelli, F.; Stratan, A.; D’Aniello, M.; Calado, L.; et al. A risk-consistent approach to determine EN1998 behaviour factors for lateral load resisting systems. *Soil Dyn. Earthq. Eng.* **2020**, *131*, 106008. [[CrossRef](#)]
44. Lagaros, N.; Papadrakakis, M. Seismic design of RC structures: A critical assessment in the framework of multi-objective optimization. *Earthq. Eng. Struct. Dyn.* **2007**, *36*, 1623–1639. [[CrossRef](#)]
45. Mergos, P. Optimum seismic design of reinforced concrete frames according to Eurocode 8 and fib Model Code 2010. *Earthq. Eng. Struct. Dyn.* **2017**, *46*, 1181–1201. [[CrossRef](#)]
46. Hernández-Montes, E.; Chatzidaki, A.; Gil-Martin, L.M.; Aschheim, M.; Vamvatsikos, D. A Seismic Design Procedure for Different Performance Objectives for Post-Tensioned Walls. *J. Earthq. Eng.* **2022**, *26*, 475–492. [[CrossRef](#)]
47. Pecker, A. Development of the second generation of Eurocode 8—Part 5: A move towards performance-based design. In *Earthquake Geotechnical Engineering for Protection and Development of Environment and Constructions, Proceedings of the 7th International Conference on Earthquake Geotechnical Engineering, Rome, Italy, 17–20 January 2019*; ISSMGE: London, UK, 2019; pp. 273–281.
48. Lombardi, L.; De Luca, F. Derivation of fragility curves at design stage through linear time-history analysis. *Eng. Struct.* **2020**, *219*, 110900. [[CrossRef](#)]
49. Cao, X.-Y.; Feng, D.-C.; Beer, M. Consistent seismic hazard and fragility analysis considering combined capacity-demand uncertainties via probability density evolution method. *Struct. Saf.* **2023**, *103*, 102330. [[CrossRef](#)]
50. Lagos, R.; Lafontaine, M.; Bonelli, P.; Boroschek, R.; Guendelman, T.; Massone, L.M.; Saragoni, R.; Rojas, F.; Yañez, F. The quest for resilience: The Chilean practice of seismic design for reinforced concrete buildings. *Earthq. Spectra* **2021**, *37*, 26–45. [[CrossRef](#)]
51. ACHISINA. *Alternative Procedure for Seismic Analysis and Design of Buildings*; Subcomité n° 7 de ACHISINA: Santiago, Chile, 2017. (In Spanish)
52. ACI. *318-08: Building Code Requirements for Structural Concrete and Commentary*; American Concrete Institute: Farmington Hills, MI, USA, 2008.
53. ACI. *318-319: Building Code Requirements for Structural Concrete and Commentary*; American Concrete Institute: Farmington Hills, MI, USA, 2019.
54. Seismosoft Ltd. *SeismoStruct 2021 User Manual—A Computer Program for Static and Dynamic Nonlinear Analysis of Framed Structures*. Pavia, Italy. 2021. [En línea]. Available online: <https://seismosoft.com/> (accessed on 1 February 2021).
55. Seismosoft Ltd. *SeismoBuild 2021 User Manual—A Computer Program for Seismic Assessment of Reinforced Concrete Framed Structures*. Pavia, Italy. 2021. Available online: <https://seismosoft.com/> (accessed on 1 February 2021).
56. Cao, X.-Y.; Chong, C.-Z.; Feng, D.-C.; Wu, G. Dynamic and probabilistic seismic performance assessment of precast prestressed reinforced concrete frames incorporating slab influence through three-dimensional spatial model. *Bull. Earthq. Eng.* **2022**, *20*, 6705–6739. [[CrossRef](#)]
57. Vielma, J.C.; Barbat, A.H.; Oller, S. Seismic performance of buildings with waffled-slab floors. *ICE Proc. Struct. Build.* **2009**, *162*, 169–182. [[CrossRef](#)]
58. Mander, J.B.; Priestley, M.J.N.; Park, R. Theoretical Stress-Strain Model for Confined Concrete. *J. Struct. Eng.* **1988**, *114*, 1804–1826. [[CrossRef](#)]
59. Menegotto, M.; Pinto, P.E. Method of analysis for cyclically loaded R.C. plane frames including changes in geometry and nonelastic behavior of elements under combined normal force and bending. In *Proceedings of the Symposium on the Resistance and Ultimate Deformability of Structures Acted on by Well Defined Repeated Loads, International Association for Bridge and Structural Engineering, Zurich, Switzerland, 1973*; pp. 15–22.
60. Al-Atik, L.; Abrahamson, N.A. An improved method for nonstationary spectral matching. *Earthq. Spectra* **2010**, *26*, 601–617. [[CrossRef](#)]

61. Cao, X.-Y.; Feng, D.-C.; Li, Y. Assessment of various seismic fragility analysis approaches for structures excited by non-stationary stochastic ground motions. *Mech. Syst. Signal Process.* **2023**, *186*, 109838. [CrossRef]
62. Center for Engineering Strong Motion Data (CESMD). 2021. [En línea]. Available online: <https://www.strongmotioncenter.org/index.html> (accessed on 20 May 2021).
63. Arias, A. A Measure of Earthquake Intensity. In *Seismic Design for Nuclear Plants*; Hansen, R.J., Ed.; The MIT Press: Cambridge, MA, USA, 1970; pp. 438–483.
64. Seismosoft Ltd. *SeismoMatch 2020 User Manual—SeismoMatch 2020—A Computer Program for Spectrum Matching of Earthquake Records*; Seismosoft Ltd.: Pavia, Italy, 2020; Available online: <https://seismosoft.com/> (accessed on 12 June 2021).
65. Vielma, J.C.; Mulder, M. Improved procedure for determining the ductility of buildings under seismic loads. *Rev. Int. De Métodos Numéricos Para Cálculo Y Diseño En Ing.* **2018**, *34*, 1–27. [CrossRef]
66. Porcu, M.C.; Vielma, J.C.; Pais, G.; Osorio, D.; Vielma-Quintero, J.C. Some issues on the seismic assessment of shear-wall buildings through code-compliant dynamic analyses. *Buildings* **2022**, *12*, 694. [CrossRef]

**Disclaimer/Publisher’s Note:** The statements, opinions and data contained in all publications are solely those of the individual author(s) and contributor(s) and not of MDPI and/or the editor(s). MDPI and/or the editor(s) disclaim responsibility for any injury to people or property resulting from any ideas, methods, instructions or products referred to in the content.